Revision2

Word Count: 11751

# Formation of metallic-Cu-bearing mineral assemblages in type-3 ordinary and CO chondrites

Ye Li[1,2,3,4*], Alan E. Rubin[4,5] and 徐伟彪 (Weibiao Hsu)[1,2*]

[1] CAS Key Laboratory of Planetary Sciences, Purple Mountain Observatory, Chinese Academy of Sciences, Nanjing 210034, China

[2] CAS Center for Excellence in Comparative Planetology, Hefei 230026, China

[3] The State Key Laboratory of Planetary Science, Macau University of Science and Technology, Macau

[4] Department of Earth, Planetary & Space Sciences, University of California, Los Angeles, CA 90095-1567, USA

[5] Maine Mineral & Gem Museum

99 Main Street, P.O. Box 500, Bethel, ME 04217, USA

*Corresponding authors: Ye Li (liye@pmo.ac.cn), Weibiao Hsu (wbxu@pmo.ac.cn)

## Abstract

Studies of the new growth and re-distribution of Cu-rich phases in chondrites of different petrologic subtypes can potentially provide insights into post-accretionary parent-body processes. We present a systematic study of the distribution of Cu-rich phases and metallic Cu in Ornans-like carbonaceous chondrites (CO3) which underwent little aqueous alteration or shock (most with shock stages of S1) but exhibit a range of thermal metamorphism (subtype 3.0-3.7). A comparison to ordinary chondrites (OCs), which have undergone a larger range of shock levels, allows to constrain the relative roles of radiogenic and shock heating in the origin of Cu distribution in chondrites. We found the Cu content of Ni-rich metal and calculated bulk Cu content of CO3 chondrites (based on mass-balance calculation) show an increase from CO3.0 to CO3.2 chondrites. We speculate that some unidentified phases in the matrix account for a significant portion (nearly ~100 ppm) of the Cu budget in bulk samples of CO3.00 chondrites, while Ni-rich metal is the main Cu-carrier for CO3.2-3.7 chondrites. Within CO3.2-3.7 chondrites, Cu and Ni contents of Ni-rich metal are positively correlated, showing a systematic decrease from lower to higher subtype (~0.41 wt% Cu and ~45.0 wt% Ni in CO3.2 Kainsaz, ~0.28 wt% Cu and ~38.8 wt% Ni in CO3.7 Isna). Metallic Cu grains were found in every sample of CO3.2-3.7 chondrites, but not in any CO3.0-3.1 chondrites. Metallic Cu is (1) present at metallic-Fe-Ni-pyrrhotite interfaces, (2) associated with fine irregular pyrrhotite grains in Ni-rich-metal-pyrrhotite nodules, (3) associated with

fizzed pyrrhotite (fine-grained mixtures of irregularly shaped metal grains surrounded by pyrrhotite), (4) present at the edges of metallic Fe-Ni grains and (5) present as isolated grains. In some metallic-Cu-bearing mineral assemblages, pyrrhotite has higher Cu concentrations than adjacent Ni-rich metal and shows a drop in Cu concentration at the interface between metallic Cu and Cu-rich pyrrhotite. This implies that the precipitation of metallic Cu grains could be related to the local Cu enrichment of pyrrhotite. We consider that radiogenic heating is mainly responsible for the formation of opaque phases in CO chondrites based on the relatively slow metallographic cooling rate (~0.1-5 °C/Ma), the increasing uniformity of Ni contents in Ni-rich metal with increasing CO subtype (44.3 ± 17.3 wt% in CO3.00 to 38.8 ± 3.4 wt% in CO3.7 chondrite), and the relatively narrow range of pyrrhotite metal/sulfur ratios (~0.976-0.999). Metal/sulfur ratios of pyrrhotite grains in most CO3.2-3.7 chondrites (mean = ~0.986-0.997; except Lancé) are slightly higher than those in CO3.0-3.1 chondrites (mean = ~0.981-0.987; except Y-81020), possibly indicative of a release and re-mobilization of sulfur during progressive heating as previously reported for type-3 chondrites. In this regard, we suggest most metallic Cu grains in CO3 chondrites may have precipitated from Cu-rich pyrrhotite due to sulfidation of Fe-Ni metal during parent-body thermal metamorphism. Locally, a few metallic Cu grains associated with fizzed pyrrhotite could have formed during transient shock-heating. Both thermal and shock metamorphism could be responsible for the formation of metallic Cu.

Although the systematic decrease in the Ni contents of Ni-rich metal from subtype-3.2 to -3.8 also occurs in OCs, the average Cu contents of Ni-rich metal grains are indistinguishable among type-3 OCs of different subtypes. The paucity of metallic Cu in weakly shocked type-3 OCs could be related to (1) the relatively low bulk Cu contents of OCs and/or (2) the relatively rapid metallographic cooling rates at <500-600 °C (~1-10 °C/Ma for LL chondrites), possibly resulting from early disturbance of OC parent bodies. The intergrowth of metallic Cu and irregular pyrrhotite more commonly occurs in shocked type-4 to -6 OCs than in CO3 chondrites. This could be due to S in type-4 to -6 OCs being more mobilized due to shock heating than in unshocked CO3 chondrites. We predict that some other groups of carbonaceous chondrites (e.g., CI and CM) are less likely to produce metallic Cu due to the (1) relatively low amount of metallic Fe-Ni, (2) relatively low parent-body temperatures of ~100-300 °C, and (3) high mobility of Cu in solution for aqueously altered samples and (4) the short heating duration for metamorphosed samples.

**Key words: metallic Cu, CO3 chondrites, type-3 ordinary chondrites, thermal metamorphism, Cu-bearing minerals**

## Introduction

Copper is a moderately volatile element with a 50% condensation temperature of 1037 K (Lodders 2003) that exhibits chalcophile/siderophile behavior during planetary differentiation processes (e.g., Righter and Drake 2000; Chabot et al. 2009; Williams and Archer 2011). Copper-bearing minerals could occur as different forms in chondrites, which were formed during nebular processes, aqueous alteration and/or metamorphism after accretion. For example, Cu could be hosted by cubanite ($CuFe_2S_3$) in CI chondrites and stardust during low-temperature (<210 °C) aqueous alteration (e.g., Berger et al. 2011); it can also enter into djerfisherite ($K_6Na_9(Fe,Cu)_{24}S_{26}Cl$) in (the highly reduced) enstatite chondrites (e.g., El Goresy et al. 1988; Lin and El Goresy 2002; Ebel and Sack 2013). Copper can also occur as metallic Cu grains in chondrites that experienced complicated thermal histories (e.g., Rubin 1994, 2003; Bennett and McSween 1996; Tomkins 2009; Komorowski et al. 2012). Among all chondritic groups, ordinary chondrites (OCs) are the major group in which metallic Cu has been observed. Metallic Cu is commonly associated with metallic Fe-Ni and troilite in OCs (e.g., Duke and Brett 1965; Bryan and Kullerud 1975; Rubin and Kallemeyn 1994). Rubin (1994) systematically studied metallic-Cu-bearing mineral assemblages in OCs and suggested that metallic Cu precipitated from local shock-melted S-rich metallic Fe-Ni liquids. Rubin (2004) proposed that metallic Cu could be used as a shock indicator for OCs, indicative of shock levels reaching to at least S3. Tomkins (2009) suggested metallic-Cu-bearing mineral assemblages formed

from shock-induced metal-gas reactions. He suggested that post-shock liberated sulfur gas reacted with metallic Fe-Ni to produce secondary troilite, taenite/tetrataenite and metallic Cu during cooling. Other occurrences of metallic Cu in OCs, which have been occasionally reported, may have different origins, such as nebular condensation (metallic Cu associated with metallic Hg, Cu-sulfides and Hg-sulfides; Komorowski et al. 2012) or low-temperature (<200 °C) solid decomposition of pentlandite on parent bodies (metallic Cu intergrown with high-Co, low-Ni metal and pyrrhotite; El Goresy 2006; Chennaoui Aoudjehane et al. 2007).

The Ornans-like (CO) carbonaceous chondrites are similar to type-3 OCs, in having experienced only limited aqueous alteration during the initial stages of thermal metamorphism (CO3.00-3.1 chondrites, indicated by the presence of magnetite and Fe,Ni-carbide; Krot et al. 1997; Rubin, 2006; Simon et al. 2019). They also resemble type-3 OCs in preserving a complete low-grade metamorphic sequence and exhibiting gradual compositional redistribution and textural recrystallization during progressive heating (McSween 1977; Grossman and Brearley 2005; Huss et al. 2005). The petrologic subtypes 3.0 to 3.7 can be divided on the basis of the compositions of olivine and kamacite (Scott and Jones 1990), petrographic characteristics of amoeboid olivine aggregates (AOAs) (a.k.a. amoeboid olivine inclusions; e.g., Chizmadia et al. 2002) and structural grade of organic matter (Bonal et al. 2007). Subtypes 3.00-3.2 show systematic changes in the $Cr_2O_3$ content of ferroan olivine (Grossman and Brearley 2005; Grossman and Rubin 2006; Davidson et al. 2014; Rubin and Li 2019). Thermoluminescence (TL) intensity was also used to classify CO chondrites (defined

as subtype 3.0-3.9; Keck and Sears 1987; Sears et al. 1991; Sears 2016), which is slightly different from those from Scott and Jones (1990) and Chizmadia et al. (2002). Shock stages of carbonaceous chondrites can be assigned from S1 to S6 on the basis of shock effects in olivine (e.g., S1: sharp optical extinction; S2: undulose extinction; S3: planar fractures; Scott et al. 1992). Many CO3 chondrites are unbrecciated and only weakly shocked (most with shock stages of S1; Scott et al. 1992).

Recently, we found metallic Cu, together with pyrrhotite (we call it pyrrhotite hereafter due to the existence of Fe-site vacancies in some samples although they are compositionally close to troilite) and metallic Fe-Ni grains, in a suite of CO3 chondrites (Rubin and Li 2019). Since the CO3 chondrites were only weakly shocked, it seems that metallic Cu in CO3 chondrites could have formed by a process other than shock. Here, we evaluate the possible origin of metallic-Cu-bearing mineral assemblages in CO3 chondrites based on our new electron-probe data and X-ray elemental mapping. For comparison, we also searched for metallic Cu in weakly shocked type-3 OCs. We use these data to provide insights into secondary processes on parent bodies of CO chondrites and further predict the formation of metallic Cu in some other groups of carbonaceous chondrites.

## Samples and analytical methods

Thin sections of 10 CO3 chondrites (CO3.00 DOM 08006, CO3.05 Yamato-81020, CO3.1 DOM 08351, CO3.1 MIL 11213, CO3.2 Kainsaz, CO3.4 Felix, CO3.5 Lancé, CO3.6 Warrenton, CO3.6 Moss and CO3.7 Isna) and 12 type-3 OCs (LL3 Harper Dry

Lake 001, LL3.00 Semarkona, LL3.2 DOM 10490, L3.6 NWA 6504, LL3.6 NWA 6696, LL3.6 NWA 094, LL3.7 NWA 980, LL3.7 NWA 5026, L3.8 NWA 481, L3.8 NWA 906, H3.8 NWA 1853 and LL3.8 NWA 6582) were examined at magnifications of 50-500x with a Zeiss petrographic microscope in transmitted and reflected light to identify metallic Cu grains (throughout the thin section) and their associated mineral assemblages. Every opaque grain visible at this magnification was examined. We also double checked the shock stages for each thin section, which are consistent with previous studies. The petrologic subtypes, whole-rock shock stages, metallic-Cu-bearing mineral assemblages, number of occurrences of metallic Cu, surface areas of thin sections, modal abundances of metallic Cu, and detailed information for the thin sections (number and institution that loaned them) are listed in Table 1. Back-scattered electron (BSE) images were made with three instruments (1) the TESCAN VEGA 3 scanning electron microscope (SEM) using a 20-keV acceleration voltage at University of California, Los Angeles (UCLA), (2) the JEOL JXA-8200 electron microprobe using an acceleration voltage of 15 keV, a 15-nA current at UCLA and (3) the JEOL JXA-8230 electron microprobe using an acceleration voltage of 15 keV, a 15-nA current at Purple Mountain Observatory (PMO). X-ray elemental maps were obtained by an Oxford AZtec energy dispersive X-ray spectrometer installed on Hitachi S-3400N SEM at PMO using a 15-keV acceleration voltage. Three or four elemental maps (scanning maps) were acquired at a resolution of 1024 × 768 pixels with 30 frames (~ 1 hour for each field) for each CO3 chondrite sample. X-ray maps of Fe, S, O, Ni combined with BSE images were

used to observe different opaque mineral phases (Fig. 1). Opaque mineral compositions were characterized with the JEOL JXA-8200 electron microprobe at UCLA using an acceleration voltage of 15 kV, a 15-nA sample current, a focused beam and 30-s counting times for Cu and 20-s counting times for other elements. The standards were chromite for Cr, forsterite for Mg and Si, millerite for S, Ni-bearing alloy NBS1156 for Ni, 99.99% pure-iron, cobalt and copper metal for Fe, Co and Cu, respectively. Compositional profiles across metal and sulfide grains were made with the microprobe using a 1-μm-diameter electron beam with spacing of 1 μm between analyzed points. The Co concentrations in metallic Fe-Ni grains were corrected for the overlap of the Fe-$K_{\beta}$ peak on the Co-$K_{\alpha}$ peak after analyzing a 99.99% iron standard. Detection limits are 0.02 wt% for Si, Mg and S, 0.04 wt% for Ni, Cr and Fe, and 0.06 wt% for Cu and Co.

## Results

### Petrography of opaque minerals and metallic-Cu-bearing mineral assemblages

**CO3.0-3.1 chondrites.** No metallic Cu grains were identified in CO3.0-3.1 chondrites. Metallic Fe-Ni and pyrrhotite grains occur both in and around chondrules (mainly FeO-poor type-I chondrules), and in the matrix. Metallic Fe-Ni grains in chondrules are spherical to ellipsoidal in shape and typically 5-60 μm in size. They are commonly rimmed (and, in some cases, fully replaced) by pyrrhotite (2-50 μm) and/or magnetite (2-80 μm), forming irregularly shaped to rounded nodules (Fig.

1a-b). These nodules also occur around some chondrules. Locally, porous polymineralic (pyrrhotite, magnetite and metallic Fe-Ni) aggregates (within which individual grains are <4 μm) are present in chondrule rims (Fig. 1a-b). In the matrix, pyrrhotite and metallic Fe-Ni grains (in some cases associated with irregular-to-round 1-80-μm-size magnetite grains) occur as spherical-to-irregular aggregates with sizes up to 200 μm (Fig. 1a-b,2a). Nickel-rich sulfide grains (mainly pentlandite) are typically associated with pyrrhotite, and, in some cases, with magnetite and Ni-rich metal (including martensite, taenite, tetrataenite and awaruite) within the matrix or inside chondrule rims in CO3.0 chondrites (Fig. 2b-c). Few Ni-rich sulfide grains were identified in CO3.1 chondrites from X-ray elemental mapping (Fig. 1b).

**CO3.2-3.7 chondrites.** Metallic Fe-Ni and pyrrhotite grains in CO3.2-3.7 chondrites occur in chondrules and the matrix. They are irregular to round in shape, present as intergrowths and isolated grains, and have larger grain sizes (up to 200-300 μm) than those in CO3.0-3.1 chondrites (Fig. 1c-f). There are far fewer opaque minerals lining chondrule surfaces in CO3.2-3.7 chondrites than in CO3.0-3.1 chondrites (Fig. 1c-f). X-ray elemental maps show few magnetite and Ni-rich sulfide grains in CO3.2-3.7 chondrites (Fig. 1c-f), consistent with previous studies (e.g., Imae and Kojima 2000; Rubin and Li 2019).

Metallic Cu grains occur in every sample of CO3.2-3.7 chondrites. Most are associated with metallic Fe-Ni and/or pyrrhotite grains in chondrule rims (37%) and within the matrix (47%); fewer grains occur in chondrule interiors (16%). Metallic Cu

grain sizes range from 1 to 13 μm, and their modal abundances are about 24.6-136.9 × $10^{-6}$ vol% (Table 1). The classification of metallic Cu petrographic assemblages in CO chondrites (e.g., Rubin 1994) can be divided into five types based on two-dimensional BSE and optical microscopic images (Table 2). Assemblages 1-3, which have relatively complex textures, are described in detail. It cannot be excluded that other mineral phases or textures occur outside the plane of the section. The metallic-Cu-bearing mineral assemblages were labelled as a dash and number after sample name (e.g., Felix-8).

**Assemblage 1: Metallic Fe-Ni-pyrrhotite interface.** This metallic-Cu-bearing mineral assemblage occurs in CO3.2 Kainsaz, CO3.4 Felix and CO3.6 Moss, in both matrix and chondrule rims. In this assemblage, metallic Fe-Ni (2-272 μm) is generally associated with or surrounded by pyrrhotite (6-100 μm in width), forming metal-pyrrhotite intergrowths (Fig. 3a-b) or nodules (Fig. 3c). Metallic Cu, generally associated with tiny Ni-rich metal grains, occurs as 2-12-μm-size irregular grains at the interface between metal and pyrrhotite (Fig. 3a-c).

**Assemblage 2: Associated with fine irregular pyrrhotite in Ni-rich metal-pyrrhotite nodules.** This metallic-Cu-bearing mineral assemblage occurs in CO3.4 Felix and CO3.6 Warrenton, in both matrix and chondrules. Nickel-rich metal-pyrrhotite nodules generally consist of Ni-rich metal (40-70 μm) and surrounding pyrrhotite rims (1-42 μm in width) (Fig. 3d-f). Metallic Cu (1-12 μm) is typically intergrown with Ni-rich metal, fine irregular pyrrhotite and kamacite (1-10 μm in width) (Fig. 3d-f). In Felix-8, the pyrrhotite rim penetrates metallic Fe-Ni,

which may be interconnected with irregular pyrrhotite grains in three dimensions (Fig. 3d). Some voids occur in the metallic Fe-Ni (Fig. 3d).

**Assemblage 3: Associated with fizzed pyrrhotite.** The intergrowth of Ni-rich metal, ragged or fizzed pyrrhotite (fine-grained mixtures of irregularly shaped metal grains surrounded by pyrrhotite), and finely irregular kamacite occurs in the matrix of CO3.7 Isna. Some phosphate grains seem to appear as irregular droplets and are intergrown with Ni-rich metal; locally, Ni-rich sulfide grain also occurs. One metallic Cu grain that contains a chromite inclusion is associated with fizzed pyrrhotite within Ni-rich metal (Fig. 3g).

Metallic Cu also occurs at the edges of metallic Fe-Ni grains (Assemblage 4; Fig. 3h) or as isolated grains (Assemblage 5; Fig. 3i). Assemblage 4 occurs in CO3.4 Felix, CO3.5 Lancé, CO3.6 Moss and CO3.7 Isna, and exits in all textural settings (i.e., matrix, chondrule rims and chondrules); Assemblage 5 occurs in chondrule rims in CO3.4 Felix.

## Type-3 ordinary chondrites

Twelve ordinary-chondrite samples of shock stage ≤S2 were examined for metallic Cu (Table 1). We confirm the absence of any metallic-Cu grains with sizes >1 μm.

The systematic changes in grain size and types of opaque minerals in type-3 OCs are similar to those in CO3 chondrites. In LL3.00 Semarkona, opaque minerals, including metallic Fe-Ni, pyrrhotite and magnetite, occur as intergrowths or as isolated grains in chondrule interiors, chondrule rims and matrix (Fig. 4a). Nickel-rich sulfide in Semarkona has been reported by many authors (e.g., Taylor et al. 1981;

Krot et al. 1997; Rubin 2006; Schrader and Zega 2019). In type-3.2 to -3.8 OCs, relatively coarse metallic Fe-Ni and pyrrhotite grains occur mainly as isolated grains and intergrowths in the matrix. Fewer grains are present around chondrules (Fig. 4b). Magnetite also occurs in OCs of higher subtypes (3.2-3.8; Fig. 4c).

**Mineral compositions**

The centers of >1-μm-size pyrrhotite (Table 3), kamacite (Supplemental Table S1) and Ni-rich metal grains (Table 4) were analyzed randomly for all the CO chondrites in this study as well as representative OCs (Table 5-6, Supplemental Table S1) to yield rough estimates of the compositions of different subtypes. Individual analyses are available in Supplemental Table S1-3. In addition, analyses were made for Ni-rich sulfide grains that had been identified on X-ray elemental maps (Table 3, Supplemental Table S2).

**Pyrrhotite metal/sulfur ratios in type-3 chondrites.** Pyrrhotite ($Fe_{1-x}S$) is a nonstoichiometric iron sulfide with x typically between 0 and 0.125. Pyrrhotite grains from CO3 chondrites have average metal/sulfur ratios (M/S, M = nFe+nCo+nNi+nCu, n in moles) of 0.975-1.000; M/S ratios of pyrrhotite grains in most CO3.2-3.7 chondrites (mean = ~0.986-0.997; except Lancé) are slightly higher than those in CO3.0-3.1 chondrites (mean = ~0.981-0.987; except Y-81020). Pyrrhotite grains from type-3 chondrites have average M/S ratios of 0.988-1.004; combined with the pyrrhotite results in Semarkona from Schrader and Zego (2019), the M/S ratios of

pyrrhotite grains in LL3.2-3.8 chondrites (mean = ~0.988-0.991) are slightly higher than those in LL3.00 chondrites (mean = ~0.986).

**Ni and Cu contents of Ni-rich metals in CO chondrites.** The Cu concentrations of kamacite, pyrrhotite and Ni-rich sulfide (which occurs only in the matrix of DOM 08006) are below the detection limit of ~0.06 wt% (Table 3, Supplemental Table S1); the Cu contents of Ni-rich metals are above the detection limit (Table 4).

In the most primitive CO3.00 chondrite (DOM 08006), the Ni contents of Ni-rich metals show a bimodal distribution with peaks at >56 wt% (tetrataenite and awaruite) and <30 wt% (taenite and martensite) that exhibit relatively wide Ni-concentration ranges with large standard deviations (Fig. 5a,6a). The petrologic subtypes versus standard deviations of Ni contents in Ni-rich metal grains in CO chondrites are shown in Supplemental Fig. S1. From subtype CO3.0 to CO3.1, the Ni contents of Ni-rich metal gradually change, with the disappearance of <35 wt% Ni-rich metal and a decrease in tetrataenite Ni content (e.g., peak at >56 wt% for CO3.00 DOM 08006; peak at ~49 wt% for CO3.1 MIL 11213) (Fig. 5a-d,6a). The average Ni contents (and the value of the Ni peaks) in Ni-rich metal grains show a systematic decrease from CO3.2 to CO3.7 (Fig. 5e-j,6a).

Nickel-rich metals in CO3.00 DOM 08006 have low Cu contents (0.09 ± 0.05 wt% Cu), lower than those in CO3.05-3.1 chondrites (0.21 ± 0.07 wt% in CO3.05 Y-81020, 0.31 ± 0.03 wt% in CO3.1 MIL 11213, 0.22 ± 0.08 wt% in CO3.1 DOM 08351; Fig. 6a). In CO3.0-3.1 chondrites, the Cu contents of Ni-rich metal in each sample are

relatively constant, and generally do not exhibit a significant correlation with the Ni contents (except for a slight negative correlation in CO3.1 DOM 08351, Fig. 6a). In CO3.2-3.7 chondrites, the Cu and Ni contents are positively correlated in Ni-rich metal: As Ni contents decrease, Cu contents decline from 0.41 ± 0.07 wt% in CO3.2 Kainsaz to 0.33 ± 0.06 wt% in CO3.5 Lancé to 0.28 ± 0.08 wt% in CO3.7 Isna (Fig. 6a).

**Ni and Cu contents of Ni-rich metals in Type-3 ordinary chondrites.** As in CO3 chondrites, Cu concentrations in type-3 OCs tend to be much higher in Ni-rich metal (Table 5) than in kamacite and pyrrhotite (<0.06 wt%, Table 6 and Supplemental Table S1).

LL3.00 Semarkona is dominated by Ni-rich metals with high Ni contents (mean = 59.3 ± 3.1 wt%) and low Cu contents (mean = 0.08 ± 0.04 wt%) (Fig. 6b and 7a). Because of the limited number of analyses, some grains with relatively low Ni contents (~10-50 wt%; Kimura et al. 2008) may have been missed. As in CO3 chondrites, Ni-rich metal grains in subtype 3.2-3.8 chondrites have lower Ni contents (average compositional range: ~37.5-46.4 wt%) and higher Cu contents (~0.21-0.27 wt%) than in type-3.0 chondrites; the average Ni contents and Ni peaks of Ni-rich metal grains show a systematic decrease from subtype 3.2 to 3.8 (Fig. 6b,7b-d). Nevertheless, Ni-rich metal in subtype 3.2-3.8 OCs have indistinguishable average Cu contents (Fig. 6b).

This is the peer-reviewed, final accepted version for American Mineralogist, published by the Mineralogical Society of America.
The published version is subject to change. Cite as Authors (Year) Title. American Mineralogist, in press.
DOI: https://doi.org/10.2138/am-2021-7689. http://www.minsocam.org/

**Metallic-Cu-bearing mineral assemblages in CO3 chondrites.** Several analyses were made on representatives of Assemblages 1-3 (Table 7 and Supplemental Table S4). We obtained 3.4-6.0 wt% Fe and 1.4-3.8 wt% Ni for most metallic Cu grains with sizes >1 μm. It is possible that the Fe contents are too high due to secondary fluorescence by Cu-Kα of Fe radiation from the adjacent metallic Fe-Ni (Olsen 1973). Kamacite grains (2.6-5.7 wt% Ni, 0.31-1.6 wt% Co) generally do not have any detectable Cu; Ni-rich metals (taenite and tetrataenite) have ~0.2-0.6 wt% Cu.

In contrast, pyrrhotite grains in the metallic-Cu-bearing mineral assemblages have variable Cu concentrations. Several compositional profiles were made traversing pyrrhotite-Ni-rich metal or pyrrhotite-metallic Cu grains. Many pyrrhotite grains contain little Cu and show no compositional variations across individual grains (e.g., Kainsaz-2, Fig. 3a and 8a; Warrenton-2; Fig. 3e and 8b). Nevertheless, there are relatively high Cu concentrations in a few pyrrhotite grains, which can exceed those in adjacent Ni-rich metal. The pyrrhotite Cu enrichment could occur (1) in the pyrrhotite-Ni-rich metal (0.61 wt%; profile 1 of Felix-11; Fig. 3c and 8c) grain boundary, (2) as irregular pyrrhotite grains enclosed by Ni-rich metal (1.0 wt% Felix-8, Fig. 3d and 8d), and (3) as grains adjacent to metallic Cu (Cu contents decrease gradually towards the far side of the pyrrhotite-metallic Cu boundary; profile 2 of Felix-11, Fig. 3c and 8e). Also, one irregular Ni-rich sulfide in Assemblage 3 of Isna-2 has a relatively high Cu content of ~0.69 wt% (Fig. 3g). There is a Cu content drop in the interface between metallic Cu and Cu-rich pyrrhotite in Felix-4 (Fig. 3b

and 8f). Some pyrrhotite grains adjacent to Ni-rich metals have relatively high Ni contents (up to ~1.0 wt%, Table 7) that gradually decrease to the far side (pyrrhotite in Fig.3c and 8e), possibly a result of diffusion.

The M/S ratios of pyrrhotite grains in the metallic-Cu-bearing mineral assemblages are basically comparable with the randomly analyzed pyrrhotite compositions. The irregular pyrrhotite grains in Ni-rich metal of Felix-1 are compositionally close to troilite (M/S ratio ~1, Table 7).

**Sulfidation states**

Method 2 from Mengason et al. (2010) (based on the chemical compositions of sulfide) was adopted to calculate the sulfur fugacity for CO3.1-3.7 chondrites that could have been redistributed during parent-body processes. The sulfur fugacity of CO3.0 chondrites that were considered the most primitive was not calculated (Davidson et al. 2019). Those of CO3.2-3.7 and CO3.1 chondrites were calculated in the temperature range of ~300-600 °C (Jones and Rubie 1991; Sears et al. 1991; Huss and Lewis 1994; Bonal et al. 2007; Imae and Nakamuta 2018) and ~100-300 °C (Zolotov et al. 2006), respectively. Sulfur fugacity is referenced to the iron-troilite (IT) buffer. Many CO3.2-3.7 chondrites (except Lancé) have slightly lower ΔIT values (IT+0.82~2.34 for most CO3.2-3.7 chondrites at ~300-600 °C) than that in CO3.1 chondrites (IT+2.31~2.91 for CO3.1 chondrites at ~100-300 °C). The sulfur fugacity relative to the iron-troilite buffer is listed in Supplemental Table S5.

362 **Metallographic cooling rate**

363 The metallographic cooling rates of CO chondrites and type-3 OCs at ~500 °C
364 were evaluated by measuring the Ni concentrations at the center of taenite grains and
365 the distance to the nearest grain boundary (Wood 1967; Willis and Goldstein 1981).
366 CO3.6 Warrenton, CO3.7 Isna and LL3.8 NWA 6582 were used to calculate cooling
367 rates because their peak temperatures could have equilibrated above ~500 °C
368 (500-600 °C for CO3.6-3.8/3.9 chondrites, Keck and Sears 1987; and 600-700 °C for
369 type-3.7 to -3.8 OCs, Wlotzka 1987; McCoy et al. 1991). Supplemental Fig. S2 shows
370 the central Ni concentrations of Ni-rich metal grains vs. distance to the nearest grain
371 boundary. The resulting metallographic cooling rates of CO3.6-3.7 chondrites
372 (Warrenton and Isna) and LL3.8 NWA 6582 are ~0.1-5 °C/Ma and ~1-10 °C/Ma,
373 respectively.

374 **Mass balance calculations**

375 CO3.00 DOM 08006, CO3.1 DOM 08351 and CO3.2 Kainsaz were used for mass
376 balance calculations. Modal abundances referred from Rubin and Li (2019) were
377 normalized to 100 vol% after excluding 0-0.45 vol% limonite; the volume ratios
378 between kamacite and Ni-rich metal were determined by X-ray elemental maps. First,
379 modal compositions were calculated from vol% to wt%; then, the mass balance of Cu
380 was estimated from the modal abundances (wt%) and Cu concentrations of
381 constituent phases. The bulk Cu contents of CO3.00 chondrite based on mass
382 calculation are around 32 ppm; the bulk Cu content of CO3.2 Kainsaz is ~135 ppm,
383 five times higher than that of CO3.00 chondrites; the bulk Cu contents of CO3.1

DOM 08351 (~52 ppm) is in between that of CO3.00 and CO3.2 chondrites. The mass balance results are shown in Supplemental Table S6.

## Discussion

### The genesis of metallic-Cu-bearing mineral assemblages in CO3 chondrites

**Could metallic Cu be a nebular product?** Previous studies found moderately volatile Cu became enriched in chondrule rims and matrix (Alexander 1995; Brearley et al. 1995) due to volatilization-recondensation (Alexander 1995) or metal/sulfide physical separation and reaccretion (Bland et al. 2005) during chondrule formation. In CO3 chondrites, most metallic Cu grains occur along with metallic Fe-Ni and/or pyrrhotite grains in chondrule rims (37%) and matrix (47%); relatively few grains of metallic Cu are present in chondrule interiors. Komorowski et al. (2012) reported metallic Cu together with metallic Hg, Cu-sulfides and Hg-sulfides in the matrix of H/L3.6 Tieschitz, and interpreted these phases as having formed by condensation followed by rapid accretion at low temperatures. Thus, a nebular origin for some metallic Cu grains seems plausible. However, we suggest that most metallic Cu grains in CO3 chondrites were formed after parent-body accretion because no metallic Cu grains were found in the most primitive CO3.0-3.1 chondrites. In this regard, we will explore Cu-bearing phases in CO chondrites as potential sources for metallic Cu.

**Matrix — a Cu reservoir in the most primitive type-3 chondrites.** In our study, pyrrhotite and metallic Fe-Ni grains (>1 μm) in the chondrules and matrix of CO3.00 DOM 08006 have low Cu concentrations (pyrrhotite, <0.06 wt% Cu; Ni-rich metal,

406 ~0.09 wt% Cu; kamacite, <0.06 wt% Cu). Also, Ni-rich sulfide (identified by
407 elemental X-ray maps) contains little Cu (<0.06 wt%) and possibly formed during
408 chondrule cooling from high temperatures (Schrader et al. 2016), sulfidation of
409 kamacite in the solar nebula (Lauretta et al. 1998) and/or as a product of
410 low-temperature aqueous alteration (Brearley 2006; Rubin 2006). Overall, no opaque
411 minerals (>1 μm) clearly enriched in Cu were observed.

412 Bulk compositions of the CO3 chondrites were calculated by mass balance, and
413 reveal that (1) the bulk Cu content of CO3.00 chondrite is five times (~32 ppm) lower
414 than that of CO3.2 Kainsaz (~135 ppm), while the calculated bulk Cu contents of
415 CO3.2 Kainsaz is comparable with previous Instrumental Neutron Activation
416 Analysis (INAA) results (~125 ppm; Wasson and Kallemeyn 1988); (2) there is a
417 corresponding increase in the Cu contents of Ni-rich metal from CO3.00 (~0.09 wt%)
418 to CO3.2 (~0.41 wt%) chondrites. This implies that some unidentified phases account
419 for a significant portion (nearly ~100 ppm) of the Cu budget in bulk CO3.00
420 chondrites, and provide Cu for Ni-rich metal during progressive parent-body heating.
421 As previously mentioned, moderately volatile Cu is concentrated in the matrix and
422 chondrule rims. Previous studies found a positive correlation between Cu and S
423 and/or Cu and Ni in matrix or chondrule rims, and suggested Ni-rich sulfide grains
424 could be the main hosts for Cu in the most primitive CO3 chondrites (Brearley 1993;
425 Alexander 1995). This is consistent with the possible decomposition of Ni-rich sulfide
426 during progressive heating, based on more Ni-rich sulfide grains in CO3.0 chondrites
427 than in CO3 chondrites of higher subtypes (Zanda et al. 1997; Bonal et al. 2007; this

428 study). However, the Cu contents in Ni-rich sulfide in our study are below the
429 detection limit. Here, we speculate that some Cu-rich nanometer-size Ni-rich sulfide
430 grains (or some similar but unknown phases), possibly embedded in matrix in CO3.0
431 chondrites, could provide Cu for Ni-rich metal during progressive heating. Further
432 high-resolution studies of fine-grained matrix in CO3.0 chondrites are required.

433 **Nickel-rich metal — the main Cu-carrier in type 3.2-3.7 chondrites.** Copper
434 tends to partition strongly into Ni-rich metal rather than into kamacite. The partition
435 coefficient of Cu between taenite and kamacite increases with the Ni content of
436 taenite (Mullane et al. 2004; Corrigan et al. 2009; Danielson et al. 2009; Meftah et al.
437 2016). These observations suggest that metallic Fe-Ni with higher Ni contents is
438 capable of incorporating more Cu than metal grains with less Ni (Danielson et al.
439 2009). This property could be a function of ionic radius (Hirata and Nesbitt 1997;
440 Meftah et al. 2016), electron configuration of the elements, or the crystal structure
441 (Hsu et al. 2000). It is supported by our electron microprobe results that Ni-rich metal
442 grains with ≥45 wt% Ni have the highest Cu contents in CO3.2-3.7 chondrites (up to
443 ~0.58 wt% Cu; Fig. 6a). The Ni-rich metal compositions of lower petrologic subtypes
444 (CO3.05-3.1) are between those of CO3.00 and CO3.2-3.7 chondrites and show an
445 unobvious or slightly positive correlation between Cu and Ni contents (Fig. 6a); this
446 implies Ni-rich metal grains in CO3.05-3.1 chondrites begin to adjust their
447 compositions at relatively low temperatures (<300 ºC; Zolotov et al. 2006), although
448 the diffusion of Cu seems to be incomplete. Metallic Cu grains in CO3.2-3.7
449 chondrites are commonly associated with metallic Fe-Ni and pyrrhotite grains. If

metallic Cu was formed by precipitation directly from Ni-rich metal, there should be local enrichments or depletions in Cu; however, our data show that Ni-rich metal grains within metallic-Cu-bearing mineral assemblages have Cu contents comparable to those analyzed randomly.

**Metallic Cu grains may have precipitated from pyrrhotite.** Although the partition coefficient of Cu between solid metal and S-bearing metallic liquid metal in Fe-Ni-S system is below 1 (Chabot et al. 2009), pyrrhotite grains (~50-355 ppm; Sutton et al. 1987) in iron meteorites and OCs (~300 ppm; Widom et al. 1986) have lower Cu contents than that in Ni-rich metal (2000-6900 ppm; Sutton et al. 1987; Kong and Ebihara 1996; Kong et al. 1998), which could be caused by subsolidus re-equilibration (Sutton et al. 1987; Kong et al. 1998). The same process may also affect CO3.2-3.7 chondrites in our study (Cu contents of pyrrhotite: <0.06 wt%; Cu contents of Ni-rich metal: ~0.28-0.41 wt%).

Nevertheless, pyrrhotite grains within metallic-Cu-bearing assemblages have variable Cu contents. Some pyrrhotite grains show a gradual Cu decrease from the metallic-Cu/Ni-rich-metal-pyrrhotite interface toward the far side (Fig. 8e). Previous studies have not reported the diffusion rate of Cu in pyrrhotite. Assuming the diffusion rate of Cu in pyrrhotite is comparable to that in chalcopyrite (Chen and Harvey 1975), we speculate that the Cu compositional gradient in these pyrrhotite grains could be due to diffusion because the diffusion rate of Cu is $10^3$-$10^4$ times faster than that of Fe at ~500 °C. Nevertheless, some pyrrhotite grains that are not directly in contact with metallic Cu have higher Cu contents than neighboring Ni-rich

472 metal grains (e.g., Felix-8; Fig. 8d). This implies that these pyrrhotite grains most
473 likely kept their pristine elemental distributions rather than having acquired them via
474 diffusion from surrounding Ni-rich metal. Local enrichment in Cu concentration,
475 which typically occurs on pyrrhotite-metallic-Fe-Ni grain boundaries (e.g., Felix-11
476 profile1; Fig. 8c), may facilitate the formation of metallic Cu. This is also consistent
477 with the drop in Cu concentration at the interface between metallic Cu and Cu-rich
478 pyrrhotite in Felix-4 having formed after the precipitation of metallic Cu (Fig. 8f).
479 Thus, the local Cu enrichment of pyrrhotite could facilitate the precipitation of
480 metallic Cu grains.

481 **Thermal metamorphism**

482 Radiogenic heating and shock heating are the two main heat sources thought
483 responsible for thermal metamorphism of asteroids. Radiogenic heating plays a major
484 role in the thermal history of chondritic parent bodies shortly after accretion
485 (Tachibana and Huss 2005; Henke et al. 2013). Shock heating could have produced
486 diverse shock and thermal effects on chondritic parent bodies throughout solar-system
487 history (Swindle et al. 2014; Stöffler et al. 2017). CO3 chondrites constitute one of
488 the least shocked chondrite groups with almost all samples being shock-stage S1
489 (Scott et al. 1992). Metallic-Cu-bearing Assemblages 1, 2, 4 and 5 occur in both
490 shocked (only Felix) and unshocked (the others) CO3 chondrites. It seems likely that
491 metallic occurrences of Fe-Ni and pyrrhotite in all the CO chondrites (including Felix)
492 were not strongly affected by shock heating because: (1) They follow the trend of
493 Ni-rich metal becoming compositionally more uniform during progressive heating

494 (Fig. 5 and Supplemental Fig. S1); (2) CO3.6 Warrenton and CO3.7 Isna have slow
495 metallographic cooling rates of ~0.1-5 ºC/Ma at ~500 ºC, consistent with the results
496 (~0.1-1 ºC/Ma) from Keck and Sears (1987); (3) Shock heating may lead to a large
497 variation of M/S ratios in pyrrhotite of OCs (M/S ratios of 0.93-0.99 for pyrrhotite
498 grains from Smyer; Rubin 2002a); in contrast, the pyrrhotite grains within each CO3
499 chondrite do not show large compositional variations (standard deviations of M/S
500 ratios ~0.005-0.013). These observations suggest that shock heating is not essential
501 for the formation of metallic Cu in CO3 chondrites. Instead, radiogenic heating
502 appears to be mainly responsible for the formation of metallic-Cu-bearing mineral
503 assemblages in CO3 chondrites.

504 Although recent studies found that many sulfides in CO3 and LL3 chondrites were
505 crystallized during chondrule cooling prior to accretion, the role of low-temperature
506 annealing and metamorphism cannot be ruled out (Schrader et al. 2016; Davidson et
507 al. 2019; Schrader and Zego 2019). Heating experiments on OCs suggest that sulfur
508 could mobilize during thermal metamorphism: it can be released from pyrrhotite,
509 especially from regions with high surface energy (crystal corners and cracks), and
510 then react with metallic Fe-Ni to form newly grown pyrrhotite (Imae 1994; Lauretta et
511 al. 1997a). These experiments are consistent with the observed redistribution of
512 sulfide during progressive heating in type-3 ordinary and CO3 chondrites, with
513 numerous tiny sulfides transforming into fewer and larger sulfide grains
514 (Bourot-Denise et al. 1997; Grossman and Brearley 2005; Huss et al. 2005) and less
515 Ni-rich sulfide grains in CO3.1-3.7 chondrites (possibly decomposed to troilite and

516 Ni-rich metal; Lauretta et al. 1997b) than in CO3.0 chondrites (Zanda et al. 1997;
517 Bonal et al. 2007; this study).

518 CO3.2-3.7 chondrites probably reached temperatures in the range of ~300-600 °C
519 (Jones and Rubie 1991; Sears et al. 1991; Bonal et al. 2007; Kimura et al. 2008; Imae
520 and Nakamuta 2018), higher than those in CO3.1 chondrites (~100-300 °C; Zolotov
521 et al. 2006). Abundant metallic Fe-Ni grains in CO3.2-3.8 chondrites were
522 decomposed from magnetite that could have formed during parent-body aqueous
523 alteration in CO3.0-3.1 chondrites (Krot et al. 1997; Imae and Kojima 2000); this
524 could be caused by increases in temperature and the $H_2/H_2O$ ratio in the gas (Zolotov
525 et al. 2006). The slightly higher M/S ratios and correspondingly lower ΔIT values in
526 CO3.2-3.7 chondrites (M/S = 0.986-0.997, ΔIT = +0.82~2.34 for most CO3.2-3.7
527 chondrites at ~300-600 °C) than those in CO3.1 chondrites (M/S = 0.986-0.987, ΔIT =
528 +2.31~2.91 at ~100-300 °C, Supplemental Table S5) support previous studies that
529 pyrrhotite could transform into troilite by releasing sulfur in chondrites (Lauretta et al.
530 1997a; Tomkins 2009):

531 $$\text{Pyrrhotite} \rightarrow \text{Troilite} + \text{Sulfur} \quad (1)$$

532 The troilite-iron buffer is bounded by the reaction:

533 $$\text{Troilite} \rightarrow \text{Metallic Fe-Ni} + \text{Sulfur} \quad (2)$$

534 Small amounts of sulfur, occurring either as $S_2$ or $H_2S$ gas, can react with metallic
535 Fe-Ni, extract Fe for pyrrhotite or troilite, and leave Ni-rich metal (Tomkins 2009).
536 The possible reaction proposed by Tomkins (2009) is:

537 $$\text{Metallic Fe-Ni} + \text{Sulfur} \rightarrow \text{Pyrrhotite/troilite} + \text{Ni-rich metal} \quad (3)$$

538 The irregular sulfide grain in Felix-1 (Table 7), with a higher M/S ratio (M/S ~1;
539 compositionally consistent with troilite) than the average M/S ratios of pyrrhotite in
540 Felix (~0.986), is supposed to form during reaction (3). The newly formed
541 pyrrhotite/troilite grains, probably locally enriched in Cu (Fig. 8d), were not in
542 equilibrium. As the reaction proceeded, metallic Cu precipitated from pyrrhotite.
543 Then, the boundary of pyrrhotite (adjacent to the precipitated grains of metallic Cu)
544 would be locally depleted in Cu relative to the surroundings (Fig. 8f).

545 **Shock-related origin**

546 Intergrowths of fizzed or ragged pyrrhotite and Ni-rich metal shown in Assemblage
547 3 (Isna-2; Fig. 3g) have been reported in many chondrites (e.g., Scott 1982; Bennett
548 and McSween 1996; Tomkins 2009); these features are likely formed by a process
549 involving rapid melting and cooling. This mechanism is consistent with the
550 occurrence of phosphate droplets and minor chromite in Ni-rich metal. During heating,
551 P and Cr originally incorporated in phosphate and chromite grains are reduced and
552 dissolved into a Fe-Ni-S melt. Phosphate and chromite grains precipitate together with
553 metal-pyrrhotite during cooling. Because of the chalcophile character of elemental Cu
554 and Cr (Chabot et al. 2010; Semenenko and Perron 2010), it seems probable that
555 metallic Cu was formed by crystallization from a S-rich metal melt (Rubin 1994),
556 most likely together with chromite (Fig. 3g). This is supported by the relatively high
557 Cu contents (0.69 wt%) in Ni-rich sulfide from Isna-2 as well as in OCs that
558 experienced relatively high-temperature processes (e.g., up to 0.88 wt% Cu in

559 pyrrhotite from LL5 Chelyabinsk; up to 0.66 wt% Cu in pyrrhotite from LL6 Appley
560 Bridge; Schrader and Zega 2019). The formation of the fizzed texture could be related
561 to post-shock metamorphism after melting (>850 °C; Tomkins 2009) or
562 recrystallization of a metallic glass (Scott 1982) formed during a shock-related
563 melting process (Scott 1982; Rubin 1994). The occurrence of fizzed texture in CO3.7
564 Isna (shock-stage S1, cooling rate of ~0.1-5 ºC/Ma) and CO3.5 Lancé (shock-stage
565 S1; Scott et al. 1992) implies that local transient heating may have been common on
566 the CO parent asteroid.

567 **A comparison of metallic Cu growth between CO3 chondrites and OCs**

568 **Lack of metallic Cu in weakly shocked type-3 OCs.** It is widely accepted that
569 type-3 ordinary and CO chondrites experienced similar metamorphic effects, recorded
570 by a sequence of petrologic subtypes ranging from 3.00 to 3.7 or 3.8 (Grossman and
571 Brearley 2005). The occurrence of magnetite in some type-3 ordinary and CO
572 chondrites, especially in low subtypes, suggests these chondrites experienced aqueous
573 alteration and oxidation at a very early stage of thermal metamorphism (Choi et al.
574 1997; Krot et al. 1997). During progressive heating, these rocks underwent textural
575 recrystallization, increases in the FeO contents of mafic minerals, decreases in the Cr
576 contents of olivine, and mobilization of S and alkalis (Scott and Jones 1990; Grossman
577 and Brearley 2005). They also exhibit increasing coarsening of Ni-rich-metal grains,
578 reductions in grain-number density (Kimura et al. 2008), increases in kamacite Ni
579 contents, decreases of Ni-rich-metal Ni contents, and homogenization of Fe-Ni metal

580 compositions (McSween 1977; Nagahara 1982; Scott and Jones 1990; this study).
581 These trends are broadly consistent with changes in the composition and abundance of
582 metallic Fe-Ni during heating as shown in the Fe-Ni binary phase diagram (Reisener
583 and Goldstein 2003). Type-3.7 to -3.8 OCs were likely heated up to ~600-700 °C
584 (Wlotzka 1987; McCoy et al. 1991); CO chondrites probably reached temperatures in
585 the range of ~300-600 °C for CO3.2- to -3.7, equivalent to those of type-3.2 to -3.5 OCs
586 (Jones and Rubie 1991; Sears et al. 1991; Huss and Lewis 1994; Bonal et al. 2007; Imae
587 and Nakamuta 2018).

588 Unlike the occurrences of metallic Cu in CO3.2-3.7 chondrites,
589 unshocked-to-weakly shocked type-3 OCs contain few metallic Cu grains. Only Prairie
590 Dog Creek (H3.6, S2) and Tieschitz (H/L3.6, weakly shocked) were reported to contain
591 metallic Cu (Rubin 1994; Komorowski et al. 2012). Even so, the genesis of some
592 occurrences of metallic Cu in Tieschitz may be related to nebular condensation
593 (Komorowski et al. 2012). It may be the case that thermal metamorphism did not
594 generally facilitate the growth of metallic Cu in type-3 OCs.

595 The presence of metallic Cu is related to the bulk Cu content of the chondrites. The
596 bulk Cu content of OCs (~80-90 ppm) is lower than that of CO chondrites (~125 ppm;
597 Wasson and Kallemeyn 1988). These differences in bulk Cu are reflected in the
598 somewhat lower Cu contents of Ni-rich metal grains in type-3 OCs (up to ~0.38 wt%;
599 Fig. 6b) compared to those in CO chondrites (up to ~0.58 wt%; Fig. 6a). The relatively
600 low Cu concentration of Ni-rich metal in type-3 OCs prevented pyrrhotite that was
601 formed during metallic Fe-Ni sulfidation from reaching Cu saturation to precipitate

602 metallic Cu. In addition, type-3 OCs tend to have faster metallographic cooling rates at
603 ~500ºC (e.g., ~2-20 °C/Ma for H chondrites, Scott et al. 2014; ~1-10 °C/Ma for LL
604 chondrites, this study) than CO3 chondrites (~0.1-1 °C/Ma, Keck and Sears 1987; ~2-5
605 °C/Ma, Krot et al. 2014; ~0.1-5 °C/Ma, this study). The relatively rapid cooling rate at
606 <500-600 °C for type-3 OCs, possibly caused by early disturbance of parent bodies
607 (Taylor et al. 1987; Blackburn et al. 2017), may also be responsible for the incomplete
608 reaction between sulfur and metal and the precipitation of metallic Cu in type-3 OCs. In
609 comparison, metallic Cu in CO3 chondrites can be produced by prolonged interaction
610 between sulfur and metal through a relatively slow cooling rate (consistent with $^{26}$Al
611 as the major heat source; Krot et al. 2014).

612 **Growth of metallic Cu in type-4 to -6 OCs.** CO3 chondrites in this study and
613 previously studied OCs (Rubin 1994, 2004; Tomkins 2009) have similar
614 metallic-Cu-bearing mineral assemblages, which are basically produced by reaction (3)
615 (except Assemblage 3 of this study). Nevertheless, the most abundant metallic
616 Cu-bearing mineral assemblages are different: metallic Cu grains most commonly (39
617 out of 100 grains) occur adjacent to small troilite grains inside Ni-rich metal
618 (equivalent to Assemblage 2 in this study) in many type-4 to -6 OCs (Rubin 1994,
619 2002b, 2004); however, most metallic Cu grains in CO3 chondrites occur along grain
620 interfaces or grain edges (Assemblages 1, 4 and 5; 14 out of 19). Rubin (2004)
621 suggested that metallic Cu occurs in many type-4 to -6 OCs that may have been
622 shocked to shock stage >S3. It seems that shocked OCs that could have experienced

623 post-shock metamorphism with slow cooling are more likely to have metallic Cu than
624 quickly cooled ones. For example, Rose City, a quickly cooled H-chondrite
625 impact-melt breccia with abundant martensite grains (Rubin 1990), does not contain
626 metallic Cu (Rubin 1994); nevertheless, LL6 MIL 99301 (which could have reached
627 ~S4 and experienced post-shock annealing) contains myrmekitic plessite with
628 abundant metallic Cu (~1.8 x $10^{-4}$ vol%). Tomkins (2009) suggested that reaction (3)
629 could have occurred at high temperatures (beyond 800 °C, but below the Fe-FeS
630 melting temperature) during post-shock metamorphism, to account for the migration
631 of sulfur and formation of pyrrhotite and metallic Cu grains inside metallic Fe-Ni. The
632 fast kinetics of metal-sulfide reactions make them sensitive to thermal changes, and
633 the shock wave propagation-caused metal defects further promote sulfur diffusion.
634 This would lead to a relatively quick growth of metallic Cu in shocked OCs during
635 post-shock metamorphism (Tomkins 2009). In contrast, sulfur in CO3 chondrites, less
636 mobilized at low temperature during thermal metamorphism than in shocked OCs,
637 could limit the extent of reaction (3) and generally restrict it to the grain interface.

638 **Implications**

639 The majority of metallic Cu grains in CO chondrites are supposed to form (1) during
640 reaction between mobilized sulfur and a certain amount of metallic Fe-Ni, (2) at
641 temperatures >300 °C and (3) without the assistance of aqueous alteration that may
642 oxidize the metal. The relatively high bulk Cu contents in CO chondrites may further
643 facilitate the formation of metallic Cu; the lack of metallic Cu in weakly shocked type-3

644 OCs is likely caused by the relatively low bulk Cu contents and/or relatively rapid
645 cooling rates (~1-10 °C/Ma for LL chondrites). Both thermal and shock metamorphism
646 could be responsible for the formation of metallic Cu. Most metallic Cu in CO3
647 chondrites were formed during thermal metamorphism, and the growth of metallic Cu
648 in OCs seems to be related to shock heating and post-shock metamorphism.

649 Studies of the growth and re-distribution of Cu-rich phases for chondrites of
650 different groups and petrologic subtypes can potentially provide insights into
651 parent-body processes. It seems that some other groups of carbonaceous chondrites
652 (e.g., CI and CM), containing comparable or slightly lower bulk Cu contents than that
653 of CO chondrites (CI chondrites ~121 ppm and CM chondrites ~115 ppm, Wasson
654 and Kallemeyn 1988), are less likely to produce metallic Cu due to the (1) relatively
655 low amount of metallic Fe-Ni, (2) relatively low temperatures of ~100-300 °C and (3)
656 high mobility of Cu in solution during aqueous alteration. For example, CI chondrites,
657 the most heavily hydrated chondritic group with ~11 wt% bulk $H_2O$, consists mainly
658 of fine-grained phyllosilicates (e.g., Fe-Mg serpentines and saponite), sulfides,
659 carbonates and sulfates with essentially no metallic Fe-Ni (e.g., Tomeoka and Buseck
660 1988; Scott and Krot 2005; King et al. 2015); they did not form above 210 °C based
661 on the occurrence of cubanite ($CuFe_2S_3$), an important Cu-bearing mineral in CI
662 chondrites (e.g., Berger et al. 2011, 2015). CM chondrites (very low amount of
663 metallic Fe-Ni, most <0.25 vol%; Rubin et al. 2007) show diverse degrees of aqueous
664 alteration, with the occurrences of phyllosilicates (serpentine-tochilinite intergrowths),
665 carbonates (diverse Ca, Mg, Fe and Mn proportions) and magnetite (e.g., Browning et

al. 1996; Zolensky et al. 1997; Rubin et al. 2007; Howard et al. 2015). The alteration temperature for CM chondrites is around 50-300 °C (e.g., Zolensky et al. 1993; Verdier-Paoletti et al. 2017; Singerling and Brearley 2020). The occurrence of tochilinite ($2(Fe,Ni,Cu)_{1-x}S.n(Fe,Mg)(OH)_2$, containing ~0.23 wt% Cu) suggest that Cu had been oxidized to $Cu^{2+}$ (Palmer and Lauretta 2011). There are a few metamorphosed CM chondrites (e.g., Y-86720 and B-7904, >400-700 °C) characterized by the dehydration of phyllosilicates and the occurrence of opaque assemblages consisting of kamacite, Ni-Co-rich metal and pyrrhotite (Tomeoka et al. 1989; Kimura et al. 2011; Harries and Langenhorst 2013; Tonui et al. 2014). The rapid cooling rate with short heating duration (1-100 hours at 890 °C or $10\text{-}10^3$ days at 700 °C based on experimental studies, Nakato et al. 2008) could result in the paucity of metallic Cu grains in metamorphosed CM chondrites.

Declarations of interest: none

## Acknowledgements

The Antarctic meteorite samples studied here were kindly loaned from the Meteorite Working Group (MWG) and National Institute of Polar Research (NIPR), Felix, Warrenton, Isna and Semarkona were kindly loaned from Smithsonian Institution. We thank R. Esposito and F. T. Kyte of UCLA for technical assistance on

686 the EPMA analyses. The authors also thank J. T. Wasson for constructive suggestions
687 and M. K. Weisberg, S. Singerling and another anonymous referee for helpful reviews.
688 The associate editor A. Peslier involving a thorough review of the manuscript is
689 greatly appreciated. This work was supported by the B-type Strategic Priority
690 Program of the Chinese Academy of Sciences, Grant No. XDB41000000, the
691 National Natural Science Foundation of China (Grant No. 41973060, 41773059,
692 41873076, 42073060 and 41803051), the pre-research Project on Civil Aerospace
693 Technologies No. D020202 and No. D020302 funded by Chinese National Space
694 Administration, the Minor Planet Foundation of China, the opening fund of State Key
695 Laboratory of Lunar and Planetary Sciences (Macau University of Science and
696 Technology) (Macau FDCT grant No. 119/2017/A3) and NASA grant
697 NNG06GF95G.

698

699

700 **References:**

701 Alexander, C.M.O'D. (1995) Trace element contents of chondrule rims and
702 interchondrule matrix in ordinary chondrites. Geochimica et Cosmochimica
703 Acta, 59, 3247-3266.
704 Bennett, M.E., and McSween, H.Y. (1996) Shock features in iron-nickel metal and
705 troilite of L-group ordinary chondrites. Meteoritics and Planetary Science, 31,
706 255-264.
707 Berger, E. L., Zega, T. J., Keller, L. P., and Lauretta, D. S. (2011) Evidence for
708 aqueous activity on comet 81P/Wild 2 from sulfide mineral assemblages in
709 Stardust samples and CI chondrites. Geochimica et Cosmochimica Acta, 75,
710 3501-3513.
711 Berger, E. L., Keller, L. P., and Lauretta, D. S. (2015) An experimental study of the
712 formation of cubanite ($CuFe_2S_3$) in primitive meteorites. Meteoritics and
713 Planetary Science, 50, 1-14.

Blackburn, T., Alexander, C. M. O'D., Carlson, R., and ElkinsTanton, L. T. (2017) The accretion and impact history of the ordinary chondrite parent bodies. Geochimica et Cosmochimica Acta, 200, 201-217.

Bland, P.A., Alard, O., Benedix, G.K., Kearsley, A.T., Menzies, O.N., Watt, L.E., and Rogers, N.W. (2005) Volatile fractionation in the early solar system and chondrule/matrix complementarity. PNAS, 27, 13755-13760.

Bonal, L., Bourot-Denise, M., Quirico, E., Montagnac, G., and Lewin, E. (2007) Organic matter and metamorphic history of CO chondrites. Geochimica et Cosmochimica Acta, 71, 1605-1623.

Bourot-Denise, M., Zanda, B., and Hewins, R. H. (1997) Metamorphic Transformation of Opaque Minerals in Chondrites. Workshop on Parent Body and Nebular Modification of Chondritic Materials, Hawaii, abstract#4040.

Brearley, A.J. (1993) Matrix and fine-grained rims in the unequilibrated CO3 chondrite, ALHA77307: Origins and evidence for diverse, primitive nebular dust components. Geochimica et Cosmochimica Acta, 57, 1521-1550.

Brearley, A.J. (2006) The action of water. In D.S. Lauretta and H.Y. McSween, Jr., Eds., Meteorites and the Early Solar System, II, 587-624. University of Arizona Press, Tuscon.

Brearley, A.J., Bajt, S., and Sutton, S.R. (1995) Distribution of moderately volatile trace elements in fine-grained chondrule rims in the unequilibrated CO3 chondrite, ALH A77307. Geochimica et Cosmochimica Acta, 59, 4307-4316.

Browning, L., McSween, H., and Zolensky, M. (1996) Correlated alteration effects in CM carbonaceous chondrites. Geochimica et Cosmochimica Acta, 60, 2621-2633.

Bryan, W.B., and Kullerud, G. (1975) Mineralogy and chemistry of the Ashmore chondrite. Meteoritics, 10, 41-50.

Chabot, N.L., Saslow, S.A., McDonough, W.F., and Jones, J.H. (2009) An investigation of the behavior of Cu and Cr during iron meteorite crystallization. Meteoritics and Planetary Science, 44, 505-519.

Chen, J.H., and Harvey, W.W. (1975) Cation self-diffusion in chalcopyrite and pyrite. Metallurgical Transactions B, 6, 331-339.

Chennaoui Aoudjehane, H., El Goresy, A., and Jambon, A. (2007) The assemblage native copper, cobaltian kamacite, and troilite in ordinary chondrites: Dissociation products not related to a shock event. Meteoritics and Planetary Science, 42, A29.

Chizmadia, L., Rubin, A.E., and Wasson, J.T. (2002) Mineralogy and petrology of amoeboid olivine inclusions: evidence for CO3 parent-body aqueous alteration. Meteoritics and Planetary Science, 37, 1781-1796.

Choi, B.-G., McKeegan, K.D., Leshina, L.A., and Wasson, J.T. (1997) Origin of magnetite in oxidized CV chondrites: in situ measurement of oxygen isotope compositions of Allende magnetite and olivine. Earth and Planetary Science Letters, 146, 337-349.

Corrigan, C.M., Chabot, N.L., McCoy, T.J., McDonough, W.F., Watson, H.C., Saslow, S.A., and Ash, R.D. (2009) The iron–nickel–phosphorus system: Effects on the distribution of trace elements during the evolution of iron meteorites. Geochimica et Cosmochimica Acta, 73, 2674-2691.

Danielson, L.R., Righter, K., and Humayun, M. (2009) Trace element chemistry of Cumulus Ridge 04071 pallasite with implications for main group pallasites four others. Meteoritics and Planetary Science, 44, 1019-1032.

Davidson, J., Nittler, L.R., Alexander, C.M.O.D., and Stroud, R.M. (2014) Petrography of very primitive CO3 chondrites: Dominion Range 08006, Miller Range 07687, and four others. Lunar and Planetary Science Conference, abstract#1384.

Davidson, J., Alexander, C.M.O'D., Stroud, R.M., Busemann, H., and Nittler, L.R. (2019) Mineralogy and petrology of Dominion Range 08006: A very primitive CO3 carbonaceous chondrite. Geochimica et Cosmochimica Acta, 265, 259-278.

Duke, M.B., and Brett, R. (1965) Metallic copper in stony meteorites. U.S. Geological Survey Professional Paper, 525-B, B101-B103.

Ebel, D. S., and Sack, R. O., (2013) Djerfisherite: Nebular source of refractory potassium. Contributions to Mineralogy and Petrology, 166, 923-934.

El Goresy, A., Yabuki, H., Ehlers, K., Woolum, D., and Pernicka, E. (1988) Qingzhen and Yamato-691: a tentative alphabet for the EH chondrites. Proceedings of the NIPR Symposium on Antarctic Meteorites, 1, 65-101.

El Goresy A. (2006) Native copper in FeNi metal and the assemblage chromite plagioclase in ordinary chondrites: Discarded as shock parameters. Meteoritics and Planetary Science, 41, abstract#A204.

Grossman, J.N., and Brearley, A.J. (2005) The onset of metamorphism in ordinary and carbonaceous chondrites. Meteoritics and Planetary Science, 40, 87-122.

Grossman, J.N., and Rubin, A.E. (2006) Dominion Range 03238: a possible missing link in the metamorphic sequence of CO3 chondrites. Lunar and Planetary Science Conference, abstract#1383.

Harries, D., and Langenhorst, F. (2013) The nanoscale mineralogy of Fe, Ni sulfides in pristine and metamorphosed CM and CM/CI-like chondrites: Tapping a petrogenetic record. Meteoritics and Planetary Science, 48, 879-903.

Henke, S., Gail, H.-P., Trieloff, M., and Schwarz, W.H. (2013) Thermal evolution model for the H chondrite asteroid—instantaneous formation versus protracted accretion. Icarus, 226, 212-228.

Hirata, T., and Nesbitt, R.W. (1997) Distribution of platinum group elements and rhenium between metallic phases of iron meteorites. Earth and Planetary Science Letters, 147, 11-24.

Howard, K.T., Alexander, C.M.O'D., Schrader, D.L., and Dyl, K.A. (2015) Classification of hydrous meteorites (CR, CM and C2 ungrouped) by phyllosilicate fraction: PSD-XRD modal mineralogy and planetesimal environments. Geochimica et Cosmochimica Acta, 149, 206-222.

Hsu, W., Huss, G.R., and Wasserburg, G.J. (2000) Ion probe measurements of Os, Ir, Pt, and Au in individual phases of iron meteorites. Geochimica et Cosmochimica Acta, 64, 1133-1147.

Huss, G.R., and Lewis, R.S. (1994) Noble gases in presolar diamonds II: component abundances reflect thermal processing. Meteoritics, 29, 811-829.

Huss, G.R., Alexander, C.M.O., Palme, H., Bland, P.A., and Wasson, J.T. (2005) Genetic Relationships between Chondrules, Fine-grained Rims, and Interchondrule Matrix. In A.N. Krot, E.R.D. Scott, and B. Reipurth, Eds., Chondrites and the Protopanetary Disk, Astronomical Society of the Pacific, 341, 701-731.

Imae, N. (1994) Direct evidence of sulfidation of metallic grain in chondrites. Proceedings of the Japan Academy. Ser. B: Physical and Biological Sciences, 70, 133-137.

Imae, N., and Kojima, H. (2000) On the relationship between troilite and/or magnetite rimmed FeNi metals and subtype in CO3 chondrites. Antarctic Meteorite Research, 13, 65-77.

Imae, N., and Nakamuta, Y. (2018) A new mineralogical approach for CO3 chondrite characterization by X-ray diffraction: Identification of primordial phases and thermal history. Meteoritics and Planetary Science, 53, 232-248.

Jones, J.H., and Rubie, D.C. (1991) Thermal histories of CO3 chondrites: application of olivine diffusion modelling to parent body metamorphism. Earth and Planetary Science Letters, 106, 73-86.

Keck, B.D., and Sears, D.W.G. (1987) Chemical and physical studies of type 3 chondrites-VIII: Thermoluminescence and metamorphism in the CO chondrites. Geochimica et Cosmochimica Acta, 51, 3013-3021.

Kimura, M., Grossman, J.N., and Weisberg, M.K. (2008) Fe-Ni metal in primitive chondrites: indicators of classification and metamorphic conditions for ordinary and CO chondrites. Meteoritics and Planetary Science, 43, 1161-1177.

Kimura, M., Grossman, J.N., and Weisberg, M.K. (2011) Fe-Ni metal and sulfide minerals in CM chondrites: an indicator for thermal history. Meteoritics and Planetary Science, 46, 431-442.

King, A.J., Schofield, P.E., Howard, K.T., and Russell, S.S. (2015) Modal mineralogy of CI and CI-like chondrites by X-ray diffraction. Geochimica et Cosmochimica Acta, 165, 148-160.

Komorowski, C.C., El Goresy, A., Miyahara, M., Boudouma, O., and Ma, C. (2012) Discovery of Hg–Cu-bearing metal-sulfide assemblages in a primitive H-3 chondrite: Towards a new insight in early solar system processes. Earth and Planetary Science Letters, 349-350, 261-271.

Kong, P., and Ebihara, M. (1996) Metal phases of L chondrites: Theirformation and evolution in the nebula and in the parent body. Geochimica et Cosmochimica Acta, 61, 2667-2680.

Kong, P., Ebihara, M., and Xie, X. (1998) Reevaluation of formation of metal nodules in ordinary. Meteoritics and Planetary Science, 33, 993-998.

Krot, A.N., Zolensky, M.E., Wasson, J.T., Scott, E.R.D., Keil, K., and Ohsumi, K. (1997) Carbide-magnetite assemblages in type-3 ordinary chondrites. Geochimica et Cosmochimica Acta, 61, 219-237.

Krot, T.V., Scott, E.R.D., and Goldstein, J.I. (2014) Thermal Histories of CO3 Chondrites: Constraints on Parent Body Size and Time of Accretion. 77th Annual Meeting of the Meteoritical Society, abstract #5108.

Krot, A.N., Nagashima, K., Simon, S.B., and Ma, C. (2019) Grossite-rich refractory inclusions in carbonaceous chondrites: evidence for early generation of different O-isotope reservoirs in the protoplanetary disk and O-isotope exchange during fluid-rock interaction. Lunar and Planetary Science Conference, 50, abstract#1230.

Lauretta, D.S., Lodders, K., Fegley, B.J., and Kremser, D.T. (1997a) The origin of sulfide-rimmed metal grains in ordinary chondrites. Earth and Planetary Science Letters, 151, 289-301.

Lauretta, D.S., Lodders, K., and Fegley, B.J. (1997b) The alteration of nickel-bearing sulfides during thermal metamorphism on ordinary chondrite parent bodies. In *Workshop on Parent-body and nebular modification of chondritic materials*. (ed. M.E. Zolensky, A.N. Krot, and E.R.D. Scott), pp. 36-38. Lunar and Planetary Institute.

Lauretta, D.S., Lodders, K., and Fegley, B.J. (1998) Kamacite sulfurization in the solar nebula. Meteoritics and Planetary Science, 33, 821-833.

Lin, Y.T., and El Goresy, A.E. (2002) A comparative study of opaque phases in Qingzhen (EH3) and MacAlpine Hills 88136 (EL3): representatives of EH and EL parent bodies. Meteoritics and Planetary Science, 37, 577-599.

Lodders, K. (2003) Solar system abundances and condensation temperatures of the elements. The Astrophysical Journal, 591, 1220-1247.

McCoy, T.J., Scott, E.R.D., Jones, R.H., Keil, K., and Taylor, G.J. (1991) Composition of chondrule silicates in LL3-5 chondrites and implications for their nebular history and parent body metamorphism. Geochimica et Cosmochimica Acta, 55, 601-619.

McSween, J.H.Y. (1977) Carbonaceous chondrites of the Omans type: A metamorphic sequence. Geochimica et Cosmochimica Acta, 41, 477-491.

Meftah, N., Mostefaoui, S., Jambon, A., Guedda, E.H., and Pont, S. (2016) Minor and trace element concentrations in adjacent kamacite and taenite in the Krymka chondrite. Meteoritics and Planetary Science, 51, 696-717.

Mengason, M.J., Piccoli, P.M., and Candela, P (2010) An evaluation of the effect of copper on the estimation of sulfur fugacity ($fS_2$) from pyrrhotite composition. Economic Geology, 105, 1163-1169.

Mullane, E., Alard, O., Gounelle, M., and Russell, S.S. (2004) Laser ablation ICP-MS study of IIIAB irons and pallasites: constraints on the behaviour of highly

siderophile elements during and after planetesimal core formation. Chemical Geology, 208, 5-28.

Nagahara, H. (1982) Ni-Fe metals in the type 3 ordinary chondrites. Memoirs of the National Institute of Polar Research, 25, 86-96.

Nakato, A., Nakamura, T., Kitajima, F., and Nogouchi, T. (2008) Evaluation of dehydration mechanism during heating of hydrous asteroids based on mineralogical and chemical analysis of naturally and experimentally heated CM chondrites. Earth Planets Space 60, 855-864.

Olsen, E.J. (1973) Copper-nickel alloy in the Blansko chondrite. Meteoritics, 8, 259-261.

Palmer, E.E., and Lauretta, D.S. (2011) Aqueous alteration of kamacite in CM chondrites. Meteoritics and Planetary Science, 46, 1587-1607.

Reisener, R.J., and Goldstein, J.I. (2003) Ordinary chondrite metallography: Part 2. Formation of zoned and unzoned metal particles in relatively unshocked H, L, and LL chondrites. Meteoritics and Planetary Science, 38, 1679-1696.

Righter, K., and Drake, M.J. (2000) Metal/silicate equilibrium in the early Earth: new constraints from the volatile moderately siderophile elements Ga, Cu, P and Sn. Geochimica et Cosmochimica Acta, 64, 3581-3597.

Rubin, A.E. (1990) Kamacite and olivine in ordinary chondrites: Intergroup and intragroup relationships. Geochimica et Cosmochimica Acta, 54, 1217-1232.

Rubin, A.E. (1994) Metallic copper in ordinary chondrites. Meteoritics, 29, 93-98.

Rubin, A.E. (2002a) Smyer H-chondrite impact-melt breccia and evidence for sulfur vaporization. Geochimica et Cosmochimica Acta, 66, 699-711.

Rubin , A.E. (2002b) Post-shock annealing of Miller Range 99301 (LL6): Implications for impact heating of ordinary chondrites. Geochimica et Cosmochimica Acta, 66, 3327-3337.

Rubin, A.E. (2003) Chromite-plagioclase assemblages as a new shock indicator; implications for the shock and thermal histories of ordinary chondrites. Geochimica et Cosmochimica Acta, 67, 2695-2709.

Rubin, A.E. (2004) Postshock annealing and postannealing shock in equilibrated ordinary chondrites: Implications for the thermal and shock histories of chondritic asteroids. Geochimica et Cosmochimica Acta, 68, 673-689.

Rubin, A.E. (2006) A relict-grain-bearing porphyritic olivine compound chondrule from LL3.0 Semarkona that experienced limited remelting. Meteoritics and Planetary Science, 41, 1027-1038.

Rubin, A.E., and Kallemeyn, G.W. (1994) Pecora Escarpment 91002: A member of the new Rumuruti (R) chondrite group. Meteoritics, 29, 255-264.

Rubin, A.E., and Li, Y. (2019) Formation and destruction of magnetite in CO3 chondrites and other chondrite groups. Geochemistry, 79, 125528.

Rubin, A.E., Trigo- Rodríguez, J.M., Huber, H., and Wasson, J.T. (2007) Progressive aqueous alteration of CM carbonaceous chondrites. Geochimica et Cosmochimica Acta, 71, 2361-2382.

Schrader, D.L., and Zega, T.J. (2019) Petrographic and compositional indicators of formation and alteration conditions from LL chondrite sulfides. Geochimica et Cosmochimica Acta, 264, 165-179.

Schrader, D.L., Davidson, J., and McCoy, T.J. (2016) Widespread evidence for high-temperature formation of pentlandite in chondrites. Geochimica et Cosmochimica Acta, 189, 359-376.

Scott, E.R.D. (1982) Origin of rapidly solidified metal-troilite grains in chondrites and iron meteorites. Geochimica et Cosmochimica Acta, 46, 813-823.

Scott, E.R.D., and Jones, R.H. (1990) Disentangling nebular and asteroidal features of CO3 carbonaceous chondrite meteorites. Geochimica et Cosmochimica Acta, 54, 2485-2502.

Scott, E.R.D., and Krot, A.N. (2005) Chondrites and their components. In: Davis, A.M. (Ed.), Meteorites, Comets and Planets. Elsevier, Amsterdam, pp. 143-200.

Scott, E.R.D., Keil, K., and Stöffler, D. (1992) Shock metamorphism of carbonaceous chondrites. Geochimica et Cosmochimica Acta, 56, 4281-4293.

Scott, E.R.D., Krot, T.V., Goldstein, J.I., and Wakita, S. (2014) Thermal and impact history of the H chondrite parent asteroid during metamorphism: Constraints from metallic Fe-Ni. Geochimica et Cosmochimica Acta, 136, 13-37.

Sears, D.W.G. (2016) The CO chondrites: major recent Antarctic finds, their thermal and radiation history, and describing the metamorphic history of members of the class. Geochimica et Cosmochimica Acta, 188, 106-124.

Sears, D.W.G., Bartchelor, J.D., Lu, J., and Keck, B.D. (1991) Metamorphism of CO and CO-like chondrites and comparisons with type 3 ordinary chondrites. Fifteenth Symposium on Antarctic Meteorites. Proceedings of the NIPR Symposium, 4, 319-343.

Semenenko, V.P., and Perron, C. (2010) Shock-melted material in the Krymka LL3.1 chondrite: Behavior of the opaque minerals. Meteoritics and Planetary Science, 40, 173-185.

Simon, S.B., Krot, A.N., and Nagashima, K. (2019) Oxygen and Al-Mg isotopic compositions of grossite-bearing refractory inclusions from CO3 chondrites. Meteoritics and Planetary Science, 54, 1362-1378.

Singerling, S.A., and Brearley, A. J. (2020) Altered primary iron sulfides in CM2 and CR2 carbonaceous chondrites: Insights into parent body processes. Meteoritics and Planetary Science, 55, 496-523.

Stöffler, D., Keil, K., and Scott, E.R.D. (1991) Shock metamorphism of ordinary chondrites. Geochimica et Cosmochimica Acta, 55, 3845-3867.

Stöffler, D., Hamann, C., and Metzler, K. (2017) Shock metamorphism of planetary silicate rocks and sediments: Proposal for an updated classification system. Meteoritics and Planetary Science, 53, 5-49.

Swindle, T.D., Kring, D.A., and Weirich, J.R. (2014) $^{40}Ar/^{39}Ar$ ages of impacts involving ordinary chondrite meteorites. In F. Jourdan, D.F. Mark, and C.

Verati, Eds., Advances in $^{40}Ar/^{39}Ar$ Dating: from Archaeology to Planetary Sciences, 333-347. Geological Society, London, London.

Tachibana, S., and Huss, G.R. (2005) Sulfur isotope composition of putative primary troilite in chondrules from Bishunpur and Semarkona. Geochimica et Cosmochimica Acta, 69, 3075-3097.

Taylor, G.J., Okada, A., Scott, E.R.D., Rubin, A.E., Huss, G.R., and Keil, K. (1981) The occurrence and implications of carbide-magnetite assemblages in unequilibrated ordinary chondrites. Lunar and Planetary Science Conference, 12, 1076-1078.

Tomeoka, K., and Buseck, P.R. (1988) Matrix mineralogy of the Orgueil CI carbonaceous chondrite. Geochimica et Cosmochimica Acta, 52, 1627-1640.

Tomeoka, K., Kojima, H., and Yanai, K. (1989) Yamato-86720: A CM carbonaceous chondrite having experienced extreme aqueous alteration and thermal metamorphism. Proceedings of the NIPR Symposium on Antarctic Meteorites, 2, 55-74.

Tomkins, A.G. (2009) What metal-troilite textures can tell us about post-impact metamorphism in chondrite meteorites. Meteoritics and Planetary Science, 44, 1133-1149.

Tonui, E., Zolensky, M., Hiroi, T., Nakamura, T., Lipschutz, M.E., Wang, M.-S., and Okudaira, K. (2014) Petrographic, chemical and spectroscopic evidence for thermal metamorphism in carbonaceous chondrites I: CI and CM chondrites. Geochimica et Cosmochimica Acta, 126, 284-306.

Verdier-Paoletti, M.J., Marrocchi, Y., Avice, G., Roskosz, M., Gurenko, A., and Gounelle, M. (2017) Oxygen isotope constraints on the alteration temperatures of CM chondrites. Earth and Planetary Science Letters, 458, 273-281.

Wasson, J.T., and Kallemeyn, G.W. (1988) Compositions of Chondrites. Philosophical Transactions of the Royal Society of London. Series A, 325, 535-544.

Widom, E., Rubin, A.E., and Wasson J.T. (1986) Composition and formation of metal nodules and veins in ordinary chondrites. Geochimica et Cosmochimica Acta, 50, 1989-1995.

Williams, H.M., and Archer, C. (2011) Copper stable isotopes as tracers of metal-sulphide segregation and fractional crystallisation processes on iron meteorite parent bodies. Geochimica et Cosmochimica Acta, 75, 3166-3178.

Willis, J., and Goldstein, J.I. (1981) A revision of metallographic cooling rate curves for chondrites. Proceedings of Lunar and Planetary Science, 12B, 1135-1143.

Wlotzka, F. (1987) Equilibration temperatures and cooling rates of chondrites: a new approach (abstract). Meteoritics, 22, 529-531.

Wood, J.A. (1967) Chondrites: Their metallic minerals, thermal histories and parent planets. Icarus, 6, 1-49.

Zanda, B., Yu, Y., Bourot-Denise M., and Hewins, R. (1997) The history of metal and sulfides in chondrites. In *Workshop on Parent-body and nebular modification*

*of chondritic materials*. (ed. M.E. Zolensky, A.N. Krot, and E.R.D. Scott), pp. 68-70. Lunar and Planetary Institute.

Zolensky, M.E., Barrett, R., and Browning, L. (1993) Mineralogy and composition of matrix and chondrule rims in carbonaceous chondrites. Geochimica et Cosmochimica Acta, 57, 3123-3148.

Zolensky, M.E., Mittlefehldt, D.W., Lipschutz, M.E., Wang, M.-S., Clayton, R.N. Mayeda, T.K., Grady, M.M., Pillinger, C.T., and Barber, D. (1997) CM chondrites exhibit the complete petrologic range from type 2 to 1. Geochimica et Cosmochimica Acta, 61, 5099-5115.

Zolotov, M.Y., Mironenko, M.V., and Shock, E.L. (2006) Thermodynamic constraints on fayalite formation on parent bodies of chondrites. Meteoritics and Planetary Science, 41, 1775-1796.

Figure captions

Fig. 1. Representative BSE images of CO3 chondrites (upper part) and their corresponding combined X-ray maps (lower part). All scale bars are 250 μm. Colors for opaque minerals in X-ray maps: green-yellow refers to kamacite; bluish green refers to magnetite; blue refers to pyrrhotite; orange (relatively Ni-poor) or red (relatively Ni-rich) refer to Ni-rich metal; purple refers to Ni-rich sulfide. Some purple grains in the lower left corner of Fig.1a and lower right corner of Fig.1f are

1036 weathering products, verified by electron probe. Po = pyrrhotite; Mag = magnetite;
1037 Kam = kamacite.
1038
1039 Fig. 2. BSE images of (a) magnetite and (b-c) Ni-rich sulfide in CO3.00 DOM 08006.
1040 (a) An opaque nodule in the matrix consists of cores of metallic Fe-Ni and
1041 surrounding magnetite (Mag) and minor pyrrhotite (Po). Ni-rich sulfide grains are
1042 associated with pyrrhotite (b) and, in some cases, with magnetite (c) within the
1043 matrix.
1044
1045 Fig. 3. BSE images of metallic-Cu-bearing mineral assemblages in CO chondrites.
1046 The red arrows in BSE images represent the location of the compositional profiles of
1047 Fig. 8 and Table S4. Po = pyrrhotite; Nm = Ni-rich metal; Kam = kamacite; Pho =
1048 phosphate; Chr = chromite; Cu = metallic Cu.
1049
1050 Fig. 4. BSE images of type-3 OCs. (a) Opaque mineral grains (bright white grains in
1051 BSE images) present in chondrule interiors, chondrule rims and matrix within
1052 type-3.0 OC. (b) Opaque mineral grains mainly present in the matrix of type-3.2 to
1053 -3.8 OCs. (c) Magnetite (Mag) around metallic Fe-Ni in type-3.2 to -3.8 OCs.
1054
1055 Fig. 5. Histograms of Ni contents for Ni-rich metal in CO chondrites. Number
1056 represent the number of grains analyzed. In CO3.00 DOM 08006, the Ni contents of
1057 Ni-rich metals show a bimodal distribution with peaks at >56 wt% and <30 wt%;

1058 subtype CO3.0-3.1 chondrites gradually show a disappearance of <35 wt% Ni-rich
1059 metal and a decrease in tetrataenite Ni contents; the values of the Ni peaks decrease
1060 from ~48 wt% in CO3.2 to 38 wt% in CO3.7 chondrites.

1061

1062 Fig. 6. Cu vs. Ni contents for individual analyses of Ni-rich metals for (a) CO and (b)
1063 ordinary chondrites. Plots of the mean are shown as insets in the top right corner. In
1064 the plots of mean CO chondrites, blue, green and red circles refer to CO3.00,
1065 CO3.05-3.1 and 3.2-3.7 chondrites, respectively, and a trend line directing to the
1066 increasing of metamorphic grade is shown. Because of the limited number of analyses,
1067 it is likely that some grains with relatively low Ni contents in Semarkona (~10-50
1068 wt%, Kimura et al. 2008) were missed.

1069

1070 Fig. 7. Histograms of Ni contents for Ni-rich metal in type-3 OCs. Number represent
1071 the number of grains analyzed. Type-3.00 Semarkona grains are dominated by Ni-rich
1072 metals with high Ni contents (~59 wt%). Some grains with relatively low Ni contents
1073 of ~10-50 wt% (Kimura et al. 2008) are missing in Semarkona probably due to the
1074 limited number of analyses. The values of the Ni peaks decrease systematically from
1075 46 wt% in type-3.2 to 38 wt% in type-3.8 OCs.

1076

1077 Fig. 8. The compositional profiles along a traverse (marked as red arrows in Fig. 3, data
1078 in Table S4) across opaque grains in metallic-Cu-bearing mineral assemblages.

Different minerals labelled by red letters are separated by a black dashed line. Fig. 8a-b show pyrrhotite grains with little Cu contents; relatively high Cu concentrations could occur in a few pyrrhotite grains adjacent to Ni-rich metal (Fig. 8c), grains enclosed by Ni-rich metal as irregular crystals (Fig. 8d), and adjacent to metallic Cu (Fig. 8e). Fig. 8f shows a Cu content drop in the interface between metallic Cu and Cu-rich pyrrhotite. Po = pyrrhotite; Cu = metallic Cu; Kam = kamacite. Concentrations of Cu in Fig. 8a-d have been multiplied by a factor of 20-40 (e.g., shown as Cu [x30] in Fig. 8a).

## Appendix

Table S1 Mean compositions (with 1σ standard deviation) and individual analyses of kamacite (wt%) in CO3 and ordinary chondrites.

Table S2 Individual analyses of sulfide (wt%) in CO3 and ordinary chondrites.

Table S3 Individual analyses of Ni-rich metal (wt%) in CO3 and ordinary chondrites.

Table S4 Compositional profiles (wt%) of coexisting metallic Fe-Ni/Cu and pyrrhotite in CO3 chondrites. Location of the compositional profiles are shown in Fig. 3 and compositional profiles are plotted in Fig. 8. Measurements were conducted across grain boundaries. The step size is 1 μm. The length of profiles: 13 μm for Kainsaz-2 (Fig. 8a); 34 μm for Warrenton-2 (Fig. 8b); 21 μm for Felix-11 profile1 (Fig. 8c); 15 μm for Felix-8 (Fig. 8d); 15 μm for Felix-11 profile 2 (Fig. 8e); 13 μm for Felix-4 (Fig. 8f).

Table S5 Calculated sulfur fugacity (ΔIT) for CO3 chondrites at different temperatures.

Table S6 Mass balance calculation of Cu contents in CO3 chondrites.

Fig. S1. Standard deviation of Ni contents in Ni-rich metal from CO chondrites vs. CO subtype. The standard deviation is listed in Table 4, and the subtypes of CO samples are listed in Table 1.

Fig. S2. Plots of central Ni content vs. distance to the nearest edge for Ni-rich metal grains in CO3 chondrites and type-3 ordinary chondrites. The CO3.6 Warrenton, CO3.7 Isna and LL3.8 NWA 6582 were adopted to calculate cooling rates because their peak temperatures could have equilibrated above ~500 °C. Cooling curves are from Willis and Goldstein (1981).

This is the peer-reviewed, final accepted version for American Mineralogist, published by the Mineralogical Society of America.
The published version is subject to change. Cite as Authors (Year) Title. American Mineralogist, in press.
DOI: https://doi.org/10.2138/am-2021-7689. http://www.minsocam.org/

Table 1 Metallic Cu in CO3 chondrites and type-3 ordinary chondrites

| sample | subtype | thin section number | shock stage | metallic Cu | assemblage | no. | $mm^2$ | modal abundances in vol% x $10^{-6}$ |
|---|---|---|---|---|---|---|---|---|
| DOM 08006 | CO3.00 | 14 | S1 | N | | | 89 | |
| Yamato-81020 | CO3.05 | NIPR 56-4 | S1 | N | | | 102 | |
| DOM 08351 | CO3.1 | 6 | S1 | N | | | 208 | |
| MIL 11213 | CO3.1 | 8 | S1 | N | | | 216 | |
| Kainsaz | CO3.2 | UCLA 1870 | S1 | Y | 1 | 2 | 273 | 26.4 |
| Felix | CO3.4 | USNM 235-1 | S3 | Y | 1,2,4,5 | 10 | 380 | 103.2 |
| Lancé | CO3.5 | UCLA 350 | S1 | Y | 4 | 1 | 158 | 25.3 |
| Warrenton | CO3.6 | USNM 43-4 | S1 | Y | 2 | 1 | 122 | 24.6 |
| Moss | CO3.6 | UCLA 2386 | S2 | Y | 1,4 | 3 | 84 | 136.9 |
| Isna | CO3.7 | USNM5890-2 | S1 | Y | 3,4 | 2 | 273 | 38.5 |
| Harper Dry Lake 001 | LL3 | UCLA 823 | S2 | N | | | | |
| Semarkona | LL3.00 | USNM 1805-3 | S2 | N | | | | |
| DOM 10490 | LL3.2 | 11 | S2 | N | | | | |
| NWA 6504 | L3.6 | UCLA 2137 | S2 | N | | | | |
| NWA 6696 | LL3.6 | UCLA 2108 | S1 | N | | | | |
| NWA 094 | LL3.6 | UCLA 936 | S2 | N | | | | |
| NWA 980 | LL3.7 | UCLA 1413 | S2 | N | | | | |
| NWA 5026 | LL3.7 | UCLA 1936 | S2 | N | | | | |
| NWA 481 | L3.8 | UCLA 1064 | S2 | N | | | | |
| NWA 906 | L3.8 | UCLA 1404 | S2 | N | | | | |

This is the peer-reviewed, final accepted version for American Mineralogist, published by the Mineralogical Society of America.
The published version is subject to change. Cite as Authors (Year) Title. American Mineralogist, in press.
DOI: https://doi.org/10.2138/am-2021-7689. http://www.minsocam.org/

| | | | | |
|---|---|---|---|---|
| NWA 1853 | H3.8 | UCLA 1740 | S1 | N |
| NWA 6582 | LL3.8 | UCLA 2068 | S2 | N |

DOM and MIL samples from NASA – Johnson Space Center, Houston; Yamato-81020 from the National Institute of Polar Research, Japan; USNM sections from the Smithsonian Institution, Washington, D.C.; UCLA samples from University of California, Los Angeles

Petrologic subtypes from the following sources: Meteoritical Bulletin Database (MBD) – Moss, Harper Dry Lake 001, Semarkona, NWA 6696, NWA 094, NWA 980, NWA 5026, NWA 481, NWA 906, NWA 6582, DOM 10490; Davidson et al. (2014) – DOM 08006; Chizmadia et al. (2002) – Kainsaz, Lancé; Krot et al. (2019) – Yamato-81020; Sears (2016) – Felix, Isna, Warrenton; Rubin and Li (2019) – DOM 08351, MIL 11213; This study – NWA 6504, NWA 1853

shock stages from the following sources: Scott et al. (1992) – Yamato-81020, Kainsaz, Felix, Lancé, Warrenton; MBD – Moss, Harper Dry Lake 001, NWA 6504, NWA 6696, NWA 094, NWA 980, NWA 481, NWA 906, NWA 1853, NWA 6582; Stöffler et al. (1991) – Semarkona; This study – Isna, DOM 08006, DOM 08351, MIL 11213, DOM 10490, NWA 5026.

metallic Cu: Has metallic Cu been observed? Y=yes; N=no.

assemblage: the classification of metallic Cu-bearing assemblage refers to Table 2.

no.: number of occurrences of metallic Cu grains in each sample.

$mm^2$: surface area of available thin sections.

Table 2 Petrographic assemblages of metallic Cu

| ID | assemblage | number of occurrences |
|---|---|---|
| 1 | metallic Fe-Ni-pyrrhotite interface | 7 |
| 2 | associated with fine irregular pyrrhotite in Ni-rich metal- pyrrhotite nodule | 4 |
| 3 | associated with fizzed pyrrhotite | 1 |
| 4 | at the edge of metallic Fe-Ni grain | 6 |
| 5 | isolated metallic copper | 1 |

This is the peer-reviewed, final accepted version for American Mineralogist, published by the Mineralogical Society of America.
The published version is subject to change. Cite as Authors (Year) Title. American Mineralogist, in press.
DOI: https://doi.org/10.2138/am-2021-7689. http://www.minsocam.org/

Table 3 Mean compositions (with 1σ standard deviation) of sulfide (wt%) in CO3 chondrites

| subtype | CO3.00 | | | | | | CO3.05 | | | CO3.1 | | | CO3.1 | | | CO3.2 | | |
|---|---|---|---|---|---|---|---|---|---|---|---|---|---|---|---|---|---|---|
| sample | DOM 08006 | | | | | | Yamato-81020[a] | | | MIL 11213 | | | DOM 08351 | | | Kainsaz | | |
| mineral | pyrrhotite | | | Ni-rich sulfide | | | pyrrhotite | | | pyrrhotite | | | pyrrhotite | | | pyrrhotite | | |
| no. of grains | 7 | | | 11 | | | 3 | | | 7 | | | 5 | | | 9 | | |
| Cr | <0.04 | | | <0.04 | | | <0.04 | | | <0.04 | | | <0.04 | | | 0.04 | ± | 0.02 |
| Si | 0.02 | ± | 0.01 | 0.02 | ± | 0.02 | 0.02 | ± | 0.01 | <0.02 | | | 0.05 | ± | 0.02 | <0.02 | | |
| S | 36.7 | ± | 0.2 | 33.2 | ± | 0.4 | 36.1 | ± | 0.3 | 36.5 | ± | 0.2 | 36.5 | ± | 0.3 | 36.2 | ± | 0.3 |
| Ni | 0.10 | ± | 0.10 | 18.8 | ± | 1.5 | <0.04 | | | 0.04 | ± | 0.03 | 0.08 | ± | 0.02 | 0.07 | ± | 0.08 |
| Fe | 62.6 | ± | 0.3 | 46.2 | ± | 1.5 | 62.8 | ± | 0.3 | 62.6 | ± | 0.3 | 62.5 | ± | 0.2 | 62.8 | ± | 0.4 |
| Co | 0.08 | ± | 0.02 | 0.39 | ± | 0.12 | — | | | 0.07 | ± | 0.03 | 0.07 | ± | 0.01 | 0.06 | ± | 0.02 |
| Cu | <0.06 | | | <0.06 | | | <0.06 | | | <0.06 | | | <0.06 | | | <0.06 | | |
| Total | 99.6 | ± | 0.3 | 98.6 | ± | 0.5 | 99.0 | ± | 0.4 | 99.2 | ± | 0.3 | 99.2 | ± | 0.2 | 99.2 | ± | 0.5 |
| M/S[b] | 0.981 | ± | 0.005 | 1.115 | ± | 0.017 | 0.999 | ± | 0.008 | 0.987 | ± | 0.007 | 0.986 | ± | 0.011 | 0.997 | ± | 0.008 |

| subtype | CO3.4 | | | CO3.5 | | | CO3.6 | | | CO3.6 | | | CO3.7 | | |
|---|---|---|---|---|---|---|---|---|---|---|---|---|---|---|---|
| sample | Felix | | | Lancé | | | Moss | | | Warrenton | | | Isna | | |
| mineral | pyrrhotite | | | pyrrhotite | | | pyrrhotite | | | pyrrhotite | | | pyrrhotite | | |
| no. of grains | 7 | | | 3 | | | 5 | | | 9 | | | 11 | | |
| Cr | <0.04 | | | <0.04 | | | <0.04 | | | <0.04 | | | <0.04 | | |
| Si | 0.05 | ± | 0.09 | <0.02 | | | 0.03 | ± | 0.04 | 0.02 | ± | 0.01 | <0.02 | | |
| S | 36.4 | ± | 0.4 | 36.7 | ± | 0.2 | 36.0 | ± | 0.1 | 36.5 | ± | 0.3 | 36.4 | ± | 0.3 |
| Ni | <0.04 | | | <0.04 | | | 0.04 | ± | 0.04 | 0.04 | ± | 0.07 | 0.04 | ± | 0.03 |

This is the peer-reviewed, final accepted version for American Mineralogist, published by the Mineralogical Society of America.
The published version is subject to change. Cite as Authors (Year) Title. American Mineralogist, in press.
DOI: https://doi.org/10.2138/am-2021-7689. http://www.minsocam.org/

| | | | | | | | | | | | | | | | |
|---|---|---|---|---|---|---|---|---|---|---|---|---|---|---|---|
| Fe | 62.4 | ± | 0.4 | 62.3 | ± | 0.1 | 62.4 | ± | 0.2 | 62.6 | ± | 0.3 | 62.9 | ± | 0.1 |
| Co | 0.07 | ± | 0.03 | 0.08 | ± | 0.02 | 0.09 | ± | 0.01 | 0.07 | ± | 0.03 | <0.06 | | |
| Cu | <0.06 | | | <0.06 | | | <0.06 | | | <0.06 | | | <0.06 | | |
| Total | 99.0 | ± | 0.5 | 99.1 | ± | 0.3 | 98.6 | ± | 0.1 | 99.2 | ± | 0.4 | 99.3 | ± | 0.4 |
| M/S[b] | 0.986 | ± | 0.013 | 0.976 | ± | 0.005 | 0.998 | ± | 0.006 | 0.988 | ± | 0.008 | 0.993 | ± | 0.010 |

[a] Co content not detected for pyrrhotite in Yamato-81020.

[b] M/S refers to metal/sulfur ratio.

Mg contents for all spots below detection limit and not listed here.

Table 4 Mean compositions (with 1σ standard deviation) of Ni-rich metal (wt%) in CO3 chondrites

| subtype | CO3.00 | | | CO3.05 | | | CO3.1 | | | CO3.1 | | | CO3.2 | | |
|---|---|---|---|---|---|---|---|---|---|---|---|---|---|---|---|
| sample | DOM 08006 | | | Yamato-81020 | | | MIL 11213 | | | DOM 08351 | | | Kainsaz | | |
| no. of grains | 18 | | | 10 | | | 21 | | | 21 | | | 30 | | |
| Cr | 0.05 | ± | 0.05 | 0.11 | ± | 0.17 | 0.26 | ± | 0.25 | 0.34 | ± | 0.37 | 0.12 | ± | 0.16 |
| Si | 0.04 | ± | 0.04 | 0.02 | ± | 0.02 | 0.07 | ± | 0.12 | 0.03 | ± | 0.02 | 0.02 | ± | 0.02 |
| Ni | 44.3 | ± | 17.3 | 49.5 | ± | 7.3 | 45.6 | ± | 3.5 | 51.5 | ± | 6.9 | 45.0 | ± | 4.9 |
| Fe | 53.6 | ± | 17.4 | 49.8 | ± | 7.5 | 53.3 | ± | 3.3 | 46.8 | ± | 7.0 | 54.4 | ± | 5.2 |
| Co | 1.4 | ± | 0.8 | 0.86 | ± | 0.80 | 0.14 | ± | 0.07 | 0.87 | ± | 0.72 | 0.08 | ± | 0.04 |
| Cu | 0.09 | ± | 0.05 | 0.21 | ± | 0.07 | 0.31 | ± | 0.03 | 0.22 | ± | 0.08 | 0.41 | ± | 0.07 |
| Total | 99.5 | ± | 0.6 | 100.5 | ± | 0.8 | 99.7 | ± | 0.6 | 99.8 | ± | 0.8 | 100.0 | ± | 0.7 |
| subtype | CO3.4 | | | CO3.5 | | | CO3.6 | | | CO3.6 | | | CO3.7 | | |
| sample | Felix | | | Lancé | | | Moss | | | Warrenton | | | Isna | | |
| no. of grains | 24 | | | 29 | | | 19 | | | 23 | | | 22 | | |

This is the peer-reviewed, final accepted version for American Mineralogist, published by the Mineralogical Society of America.
The published version is subject to change. Cite as Authors (Year) Title. American Mineralogist, in press.
DOI: https://doi.org/10.2138/am-2021-7689. http://www.minsocam.org/

| | | | | | | | | | | | | | | | |
|---|---|---|---|---|---|---|---|---|---|---|---|---|---|---|---|
| Cr | 0.09 | ± | 0.20 | 0.21 | ± | 0.26 | <0.04 | | | 0.12 | ± | 0.16 | 0.07 | ± | 0.14 |
| Si | 0.02 | ± | 0.02 | 0.02 | ± | 0.02 | 0.02 | ± | 0.01 | 0.02 | ± | 0.01 | <0.02 | | |
| Ni | 44.4 | ± | 4.7 | 42.8 | ± | 5.2 | 43.1 | ± | 5.0 | 41.7 | ± | 5.7 | 38.8 | ± | 3.4 |
| Fe | 55.0 | ± | 5.1 | 55.8 | ± | 5.4 | 55.8 | ± | 5.3 | 57.3 | ± | 5.9 | 60.5 | ± | 3.6 |
| Co | 0.24 | ± | 0.13 | 0.18 | ± | 0.07 | 0.15 | ± | 0.05 | 0.44 | ± | 0.29 | 0.31 | ± | 0.21 |
| Cu | 0.34 | ± | 0.06 | 0.33 | ± | 0.06 | 0.35 | ± | 0.07 | 0.30 | ± | 0.07 | 0.28 | ± | 0.08 |
| Total | 100.1 | ± | 0.8 | 99.3 | ± | 0.6 | 99.5 | ± | 0.6 | 99.8 | ± | 0.8 | 99.9 | ± | 0.6 |

Mg contents for all spots below detection limit and not listed here.

Table 5 Mean compositions (with 1σ standard deviation) of Ni-rich metal (wt%) in type-3 ordinary chondrites

| subtype | LL3.00 | | | LL3.2 | | | LL3.6 | | | LL3.8 | | |
|---|---|---|---|---|---|---|---|---|---|---|---|---|
| sample | Semarkona[a] | | | DOM 10490 | | | NWA 6696 | | | NWA 6582 | | |
| no. of grains | 11 | | | 28 | | | 25 | | | 22 | | |
| Cr | <0.04 | | | 0.07 | ± | 0.11 | 0.04 | ± | 0.07 | 0.04 | ± | 0.06 |
| Si | <0.02 | | | 0.03 | ± | 0.01 | 0.02 | ± | 0.01 | <0.02 | | |
| Ni | 59.3 | ± | 3.1 | 46.4 | ± | 4.8 | 42.3 | ± | 10.8 | 37.5 | ± | 5.8 |
| Fe | 40.0 | ± | 3.1 | 52.8 | ± | 4.9 | 57.7 | ± | 10.7 | 62.0 | ± | 6.2 |
| Co | — | | | 0.16 | ± | 0.05 | 0.18 | ± | 0.10 | 0.17 | ± | 0.08 |
| Cu | 0.08 | ± | 0.04 | 0.27 | ± | 0.05 | 0.22 | ± | 0.08 | 0.21 | ± | 0.07 |
| Total | 99.4 | ± | 0.6 | 99.7 | ± | 0.7 | 100.5 | ± | 0.6 | 99.9 | ± | 0.8 |

[a] Co content not detected for Semarkona.

Mg contents for all spots below detection limit and not listed here.

This is the peer-reviewed, final accepted version for American Mineralogist, published by the Mineralogical Society of America.
The published version is subject to change. Cite as Authors (Year) Title. American Mineralogist, in press.
DOI: https://doi.org/10.2138/am-2021-7689. http://www.minsocam.org/

Table 6 Mean compositions (with 1σ standard deviation) of pyrrhotite (wt%) in type-3 ordinary chondrites

| subtype | LL3.00 | LL3.00 | LL3.2 | LL3.6 | LL3.8 |
|---|---|---|---|---|---|
| sample | Semarkona[a] | Semarkona[b] | DOM 10490 | NWA 6696 | NWA 6582 |
| no. of grains | 4 | 37 | 9 | 10 | 7 |
| Cr | <0.04 | 0.04 ± 0.02 | <0.04 | <0.04 | <0.04 |
| Si | <0.02 | 0.03 ± 0.03 | 0.04 ± 0.01 | 0.03 ± 0.01 | 0.02 ± 0.01 |
| S | 36.0 ± 0.3 | 36.7 ± 0.3 | 36.6 ± 0.2 | 37.0 ± 0.3 | 36.7 ± 0.3 |
| Ni | 0.06 ± 0.08 | 0.11 ± 0.19 | <0.04 | 0.04 ± 0.03 | 0.04 ± 0.05 |
| Fe | 62.9 ± 0.3 | 63.0 ± 0.4 | 63.0 ± 0.4 | 63.6 ± 0.3 | 63.2 ± 0.9 |
| Co | — | <0.09 | 0.07 ± 0.02 | 0.06 ± 0.02 | 0.07 ± 0.02 |
| Cu | <0.06 | <0.12 | <0.06 | <0.06 | <0.06 |
| Total | 99.0 ± 0.1 | 99.9 ± 0.5 | 99.8 ± 0.5 | 100.8 ± 0.3 | 100.0 ± 0.8 |
| M/S[c] | 1.004 ± 0.010 | 0.986 ± 0.010 | 0.989 ± 0.005 | 0.988 ± 0.010 | 0.992 ± 0.019 |

[a] Pyrrhotite data of Semarkona in this study, Co content not detected.

[b] Combined pyrrhotite data of Semarkona in this study and those from Schrader and Zego (2019), detection limit refers to Schrader and Zego (2019).

[c] M/S refers to metal/sulfur ratio.

Mg contents for all spots below detection limit and not listed here.

This is the peer-reviewed, final accepted version for American Mineralogist, published by the Mineralogical Society of America.
The published version is subject to change. Cite as Authors (Year) Title. American Mineralogist, in press.
DOI: https://doi.org/10.2138/am-2021-7689. http://www.minsocam.org/

Table 7 Representative mineral compositions (wt%) in metallic-Cu-bearing mineral assemblages in CO3 chondrites

| mineral | metallic Cu | | | kamacite | | Ni-rich metal | | | | |
|---|---|---|---|---|---|---|---|---|---|---|
| assemblage[a] | 1 | 1 | 2 | 1 | 3 | 1 | 2 | 2 | 3 | 3 |
| location | Kain-1 | Felix-11 | Felix-1 | Kain-2 spot 1 in Fig. 3a and 8a | Isna-2 irregular inclusion in Fig. 3g | Felix-11 profile 1 spot 5 in Fig. 3c and 8c | Felix-1 | War-2 | Isna-2 | Isna-2 |
| Cr | 0.11 | <0.04 | <0.04 | 0.07 | <0.04 | 0.45 | <0.04 | 0.06 | <0.04 | 0.49 |
| Si | <0.02 | 0.05 | 0.10 | 0.03 | 0.06 | 0.11 | 0.09 | 0.06 | <0.02 | 0.05 |
| Ni | 1.4 | 2.3 | 3.8 | 3.8 | 2.6 | 40.3 | 44.3 | 37.6 | 40.5 | 32.6 |
| Fe | 5.9 | 5.0 | 6.0 | 96.4 | 96.6 | 58.8 | 54.0 | 61.5 | 59.0 | 65.7 |
| Co | <0.06 | <0.06 | <0.06 | 0.38 | 1.1 | 0.22 | 0.24 | 0.27 | 0.41 | 0.53 |
| Mg | 0.07 | <0.02 | <0.02 | <0.02 | 0.04 | <0.02 | <0.02 | <0.02 | <0.02 | <0.02 |
| Cu | 93.3 | 87.7 | 90.6 | <0.06 | <0.06 | 0.24 | 0.49 | 0.22 | 0.24 | 0.20 |
| Total | 100.8 | 95.0 | 100.4 | 100.7 | 100.4 | 100.1 | 99.2 | 99.8 | 100.1 | 99.6 |

| mineral | pyrrhotite | | | | | | | | |
|---|---|---|---|---|---|---|---|---|---|
| assemblage[a] | 1 | 1 | 1 | 2 | 2 | 2 | 2 | 3 | 3 |
| location | Kain-2 | Felix-11 profile 2 | Felix-11 profile 2 | Felix-8 | Felix-11 profile 1 | Felix-1 | War-2 | Isna-2 | Isna-2 |

This is the peer-reviewed, final accepted version for American Mineralogist, published by the Mineralogical Society of America.
The published version is subject to change. Cite as Authors (Year) Title. American Mineralogist, in press.
DOI: https://doi.org/10.2138/am-2021-7689. http://www.minsocam.org/

| | spot 9 in Fig. 3a and 8a | spot 5 in Fig. 3c and 8e | spot 15 in Fig. 3c and 8e | spot 8 in Fig. 3d and 8d | spot 12 in Fig. 3c and 8c | irregular inclusion in Fig. 3f | spot 4 in Fig.3e and 8b | irregular inclusion in Fig. 3g | ragged rims in Fig. 3g |
|---|---|---|---|---|---|---|---|---|---|
| Cr | <0.04 | <0.04 | <0.04 | <0.04 | <0.04 | <0.04 | <0.04 | <0.04 | <0.04 |
| Si | 0.04 | 0.07 | 0.12 | 0.10 | 0.13 | 0.13 | 0.13 | 0.06 | 0.08 |
| S | 35.7 | 35.7 | 36.0 | 36.1 | 35.7 | 36.4 | 36.5 | 33.1 | 36.3 |
| Ni | 0.15 | 0.33 | 0.06 | 0.49 | 0.34 | 0.88 | 0.15 | 5.1 | 0.67 |
| Fe | 64.1 | 61.5 | 61.6 | 61.1 | 59.7 | 62.4 | 62.3 | 59.4 | 62.8 |
| Co | <0.06 | 0.07 | 0.08 | 0.10 | 0.08 | <0.06 | <0.06 | 0.11 | <0.06 |
| Mg | <0.02 | <0.02 | 0.02 | <0.02 | <0.02 | <0.02 | <0.02 | 0.02 | 0.02 |
| Cu | <0.06 | 0.96 | 0.07 | 1.0 | 0.61 | 0.06 | <0.06 | 0.69 | <0.06 |
| Total | 100.0 | 98.7 | 98.0 | 98.9 | 96.6 | 99.9 | 99.0 | 98.5 | 99.9 |
| M/S[b] | 1.033 | 1.008 | 0.984 | 0.993 | 0.974 | 0.998 | 0.982 | 1.115 | 1.003 |

[a] assemblage numbers refer to those in Table 2.

[b] M/S refers to metal/sulfur ratio.

abbreviation: Kain = Kainsaz; War = Warrenton

Figure 1

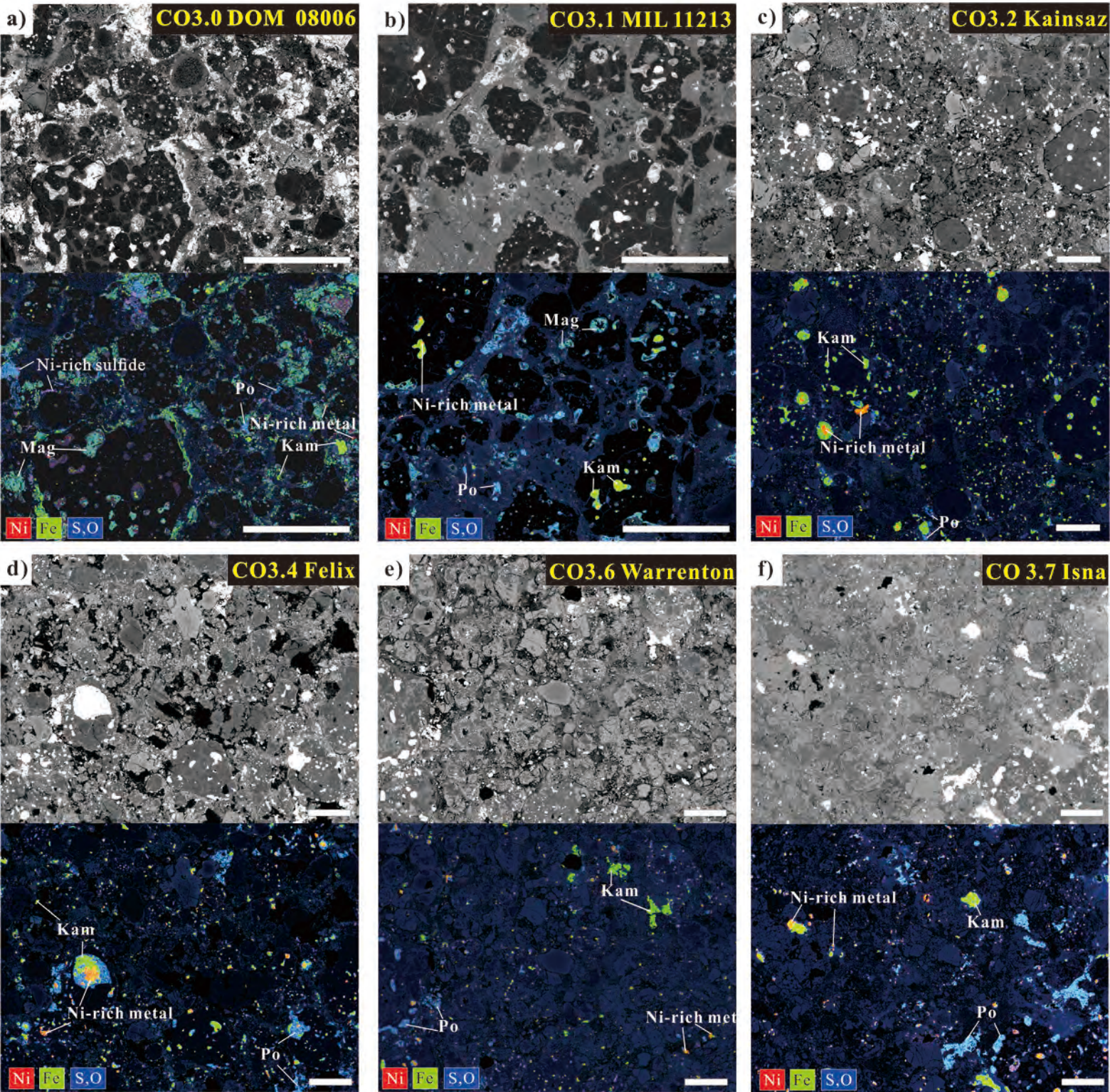
a)
CO3.0 DOM 08006
Ni-rich sulfide
Po
Ni-rich metal
Mag
Kam
Ni Fe S,O
b)
CO3.1 MIL 11213
Mag
Ni-rich metal
Kam
Po
Ni Fe S,O
c)
CO3.2 Kainsaz
Kam
Ni-rich metal
Po
Ni Fe S,O
d)
CO3.4 Felix
Kam
Ni-rich metal
Po
Ni Fe S,O
e)
CO3.6 Warrenton
Kam
Po
Ni-rich met
Ni Fe S,O
f)
CO 3.7 Isna
Ni-rich metal
Kam
Po
Ni Fe S,O

Figure 2

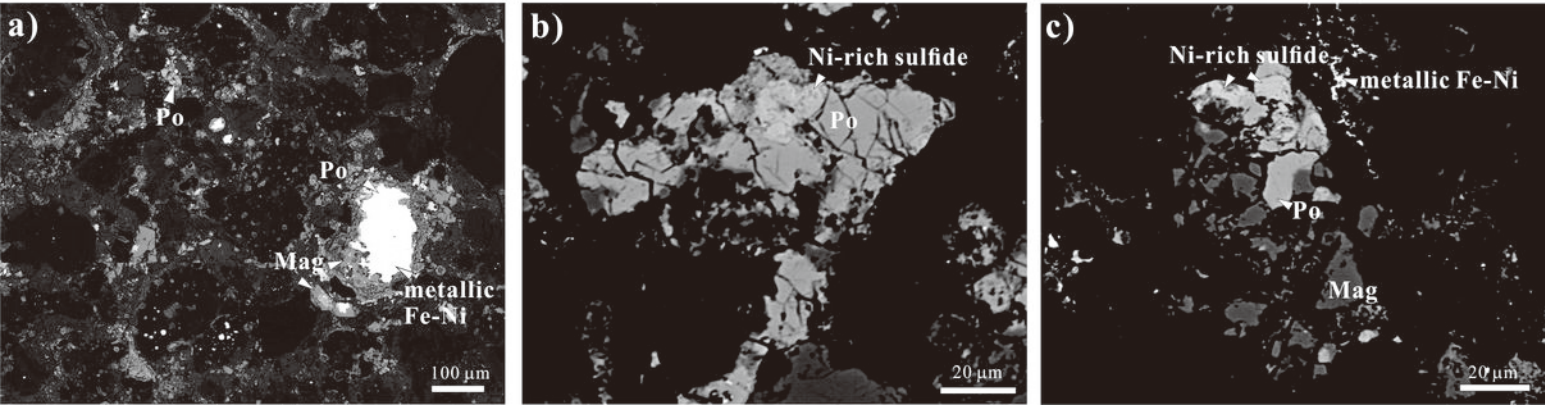
a)
Po
Po
Mag
metallic
Fe-Ni
100 μm
b)
Ni-rich sulfide
Po
20 μm
c)
Ni-rich sulfide
metallic Fe-Ni
Po
Mag
20 μm

Figure 3

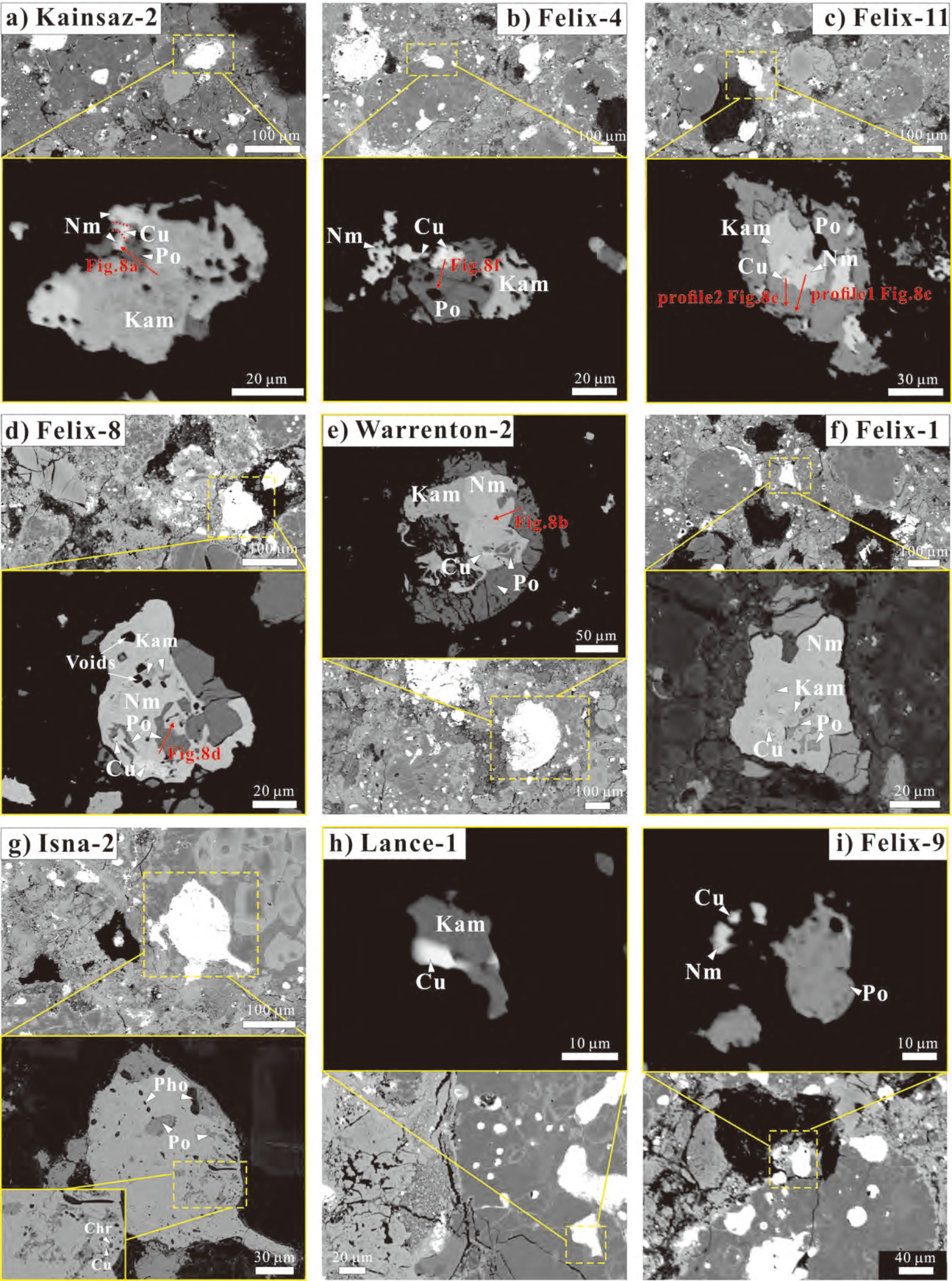
a) Kainsaz-2
100 µm
Nm
Cu
Po
Fig.8a
Kam
20 µm
b) Felix-4
100 µm
Nm
Cu
Fig.8f
Kam
Po
20 µm
c) Felix-11
100 µm
Kam
Po
Cu
Nm
profile2 Fig.8c
profile1 Fig.8c
30 µm
d) Felix-8
100 µm
Kam
Voids
Nm
Po
Fig.8d
Cu
20 µm
e) Warrenton-2
Kam
Nm
Fig.8b
Cu
Po
50 µm
100 µm
f) Felix-1
100 µm
Nm
Kam
Po
Cu
20 µm
g) Isna-2
100 µm
Pho
Po
Chr
Cu
30 µm
h) Lance-1
Kam
Cu
10 µm
20 µm
i) Felix-9
Cu
Nm
Po
10 µm
40 µm

Figure 4

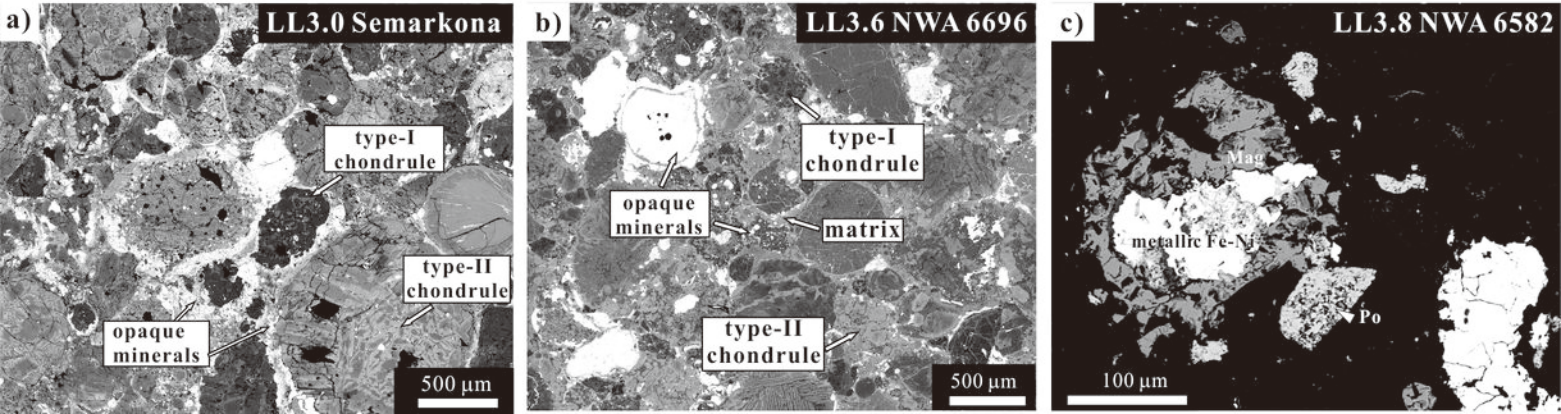
a)
LL3.0 Semarkona
type-I chondrule
type-II chondrule
opaque minerals
500 μm
b)
LL3.6 NWA 6696
type-I chondrule
opaque minerals
matrix
type-II chondrule
500 μm
c)
LL3.8 NWA 6582
Mag
metallic Fe-Ni
Po
100 μm

Figure 5

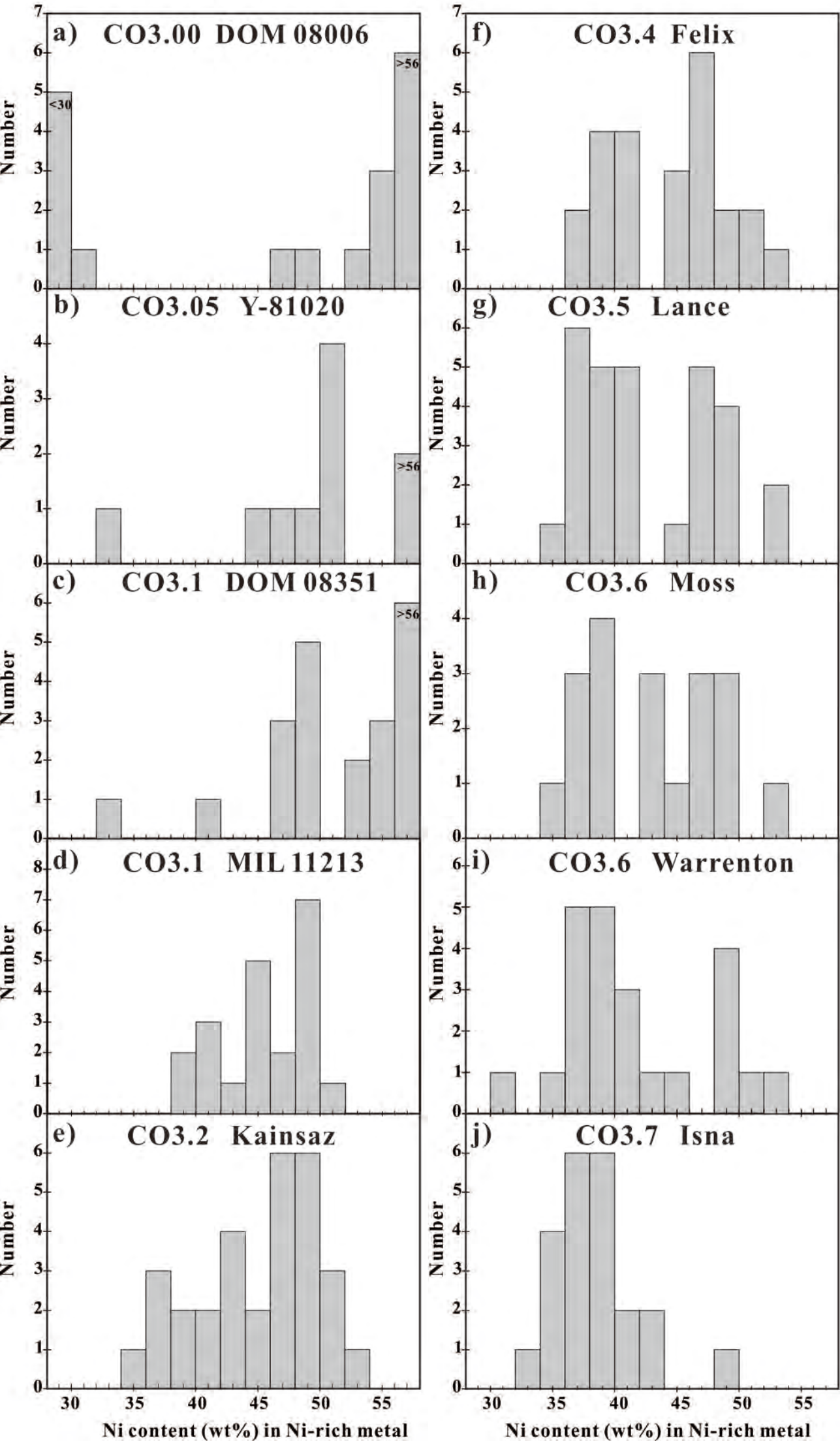
a) CO3.00 DOM 08006
<30
>56
b) CO3.05 Y-81020
>56
c) CO3.1 DOM 08351
>56
d) CO3.1 MIL 11213
e) CO3.2 Kainsaz
f) CO3.4 Felix
g) CO3.5 Lance
h) CO3.6 Moss
i) CO3.6 Warrenton
j) CO3.7 Isna
Number
Ni content (wt%) in Ni-rich metal

Figure 6

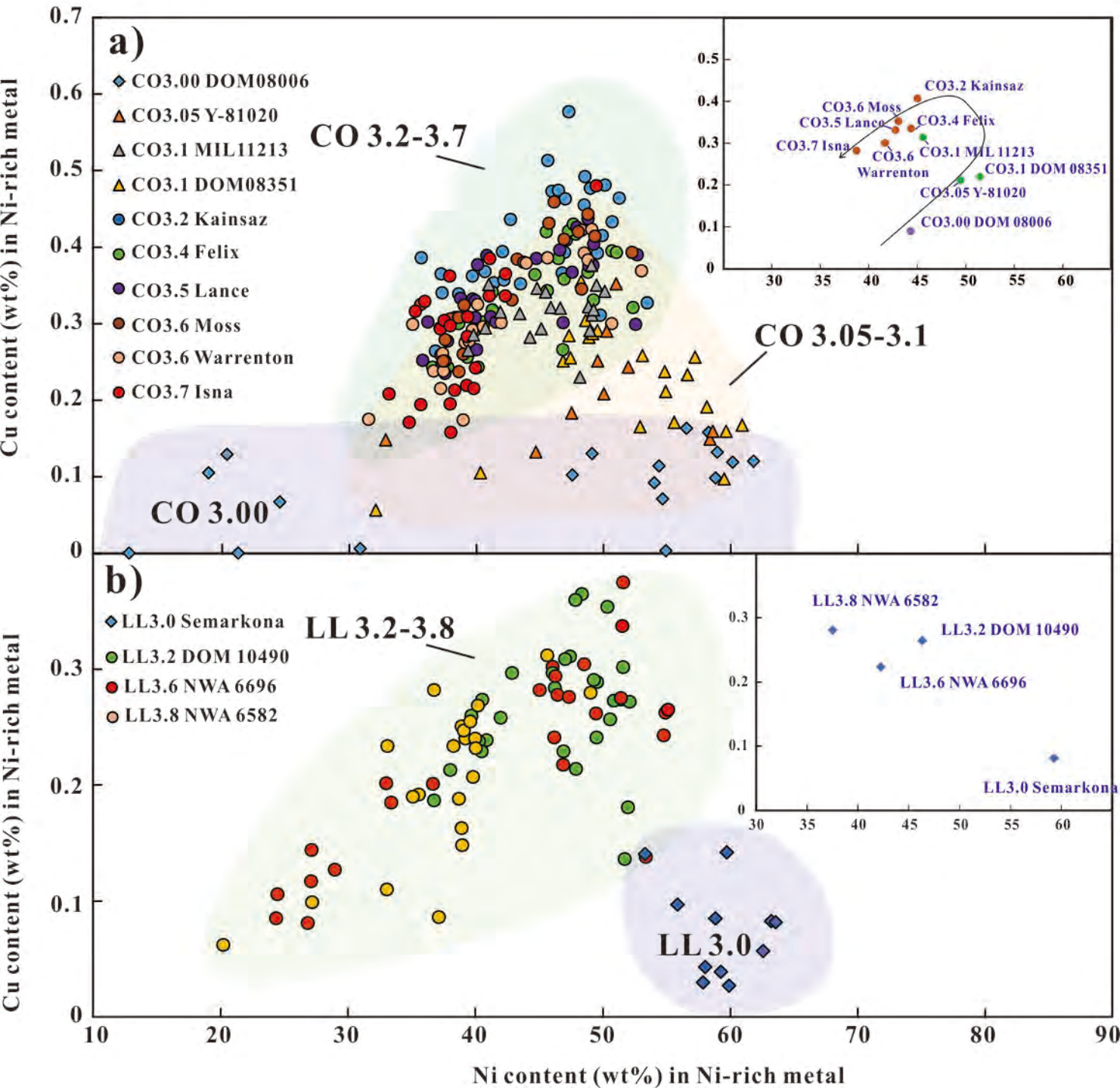
a)
CO3.00 DOM08006
CO3.05 Y-81020
CO3.1 MIL11213
CO3.1 DOM08351
CO3.2 Kainsaz
CO3.4 Felix
CO3.5 Lance
CO3.6 Moss
CO3.6 Warrenton
CO3.7 Isna
CO 3.2-3.7
CO 3.05-3.1
CO 3.00
CO3.2 Kainsaz
CO3.6 Moss
CO3.5 Lance
CO3.4 Felix
CO3.7 Isna
CO3.6
CO3.1 MIL 11213
Warrenton
CO3.1 DOM 08351
CO3.05 Y-81020
CO3.00 DOM 08006
b)
LL3.0 Semarkona
LL3.2 DOM 10490
LL3.6 NWA 6696
LL3.8 NWA 6582
LL 3.2-3.8
LL 3.0
LL3.8 NWA 6582
LL3.2 DOM 10490
LL3.6 NWA 6696
LL3.0 Semarkona
Cu content (wt%) in Ni-rich metal
Cu content (wt%) in Ni-rich metal
Ni content (wt%) in Ni-rich metal

Figure 7

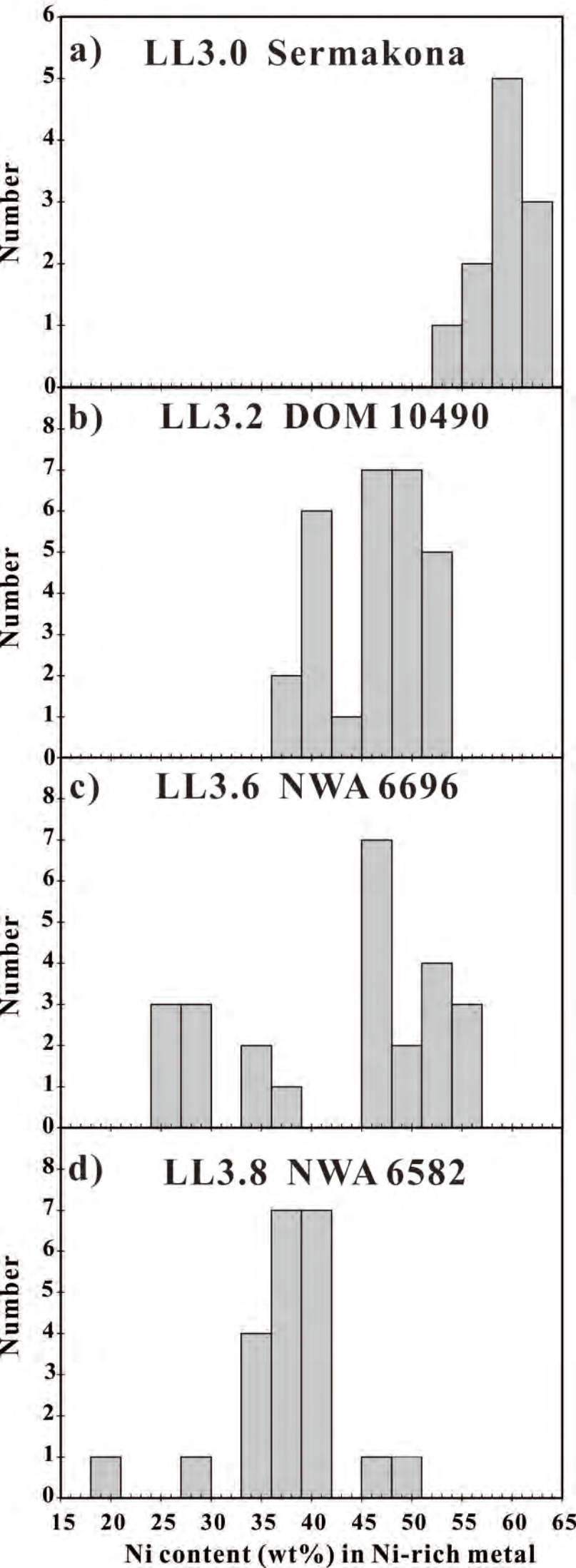
a) LL3.0 Sermakona
b) LL3.2 DOM 10490
c) LL3.6 NWA 6696
d) LL3.8 NWA 6582
Number
Ni content (wt%) in Ni-rich metal
15 20 25 30 35 40 45 50 55 60 65

Figure 8

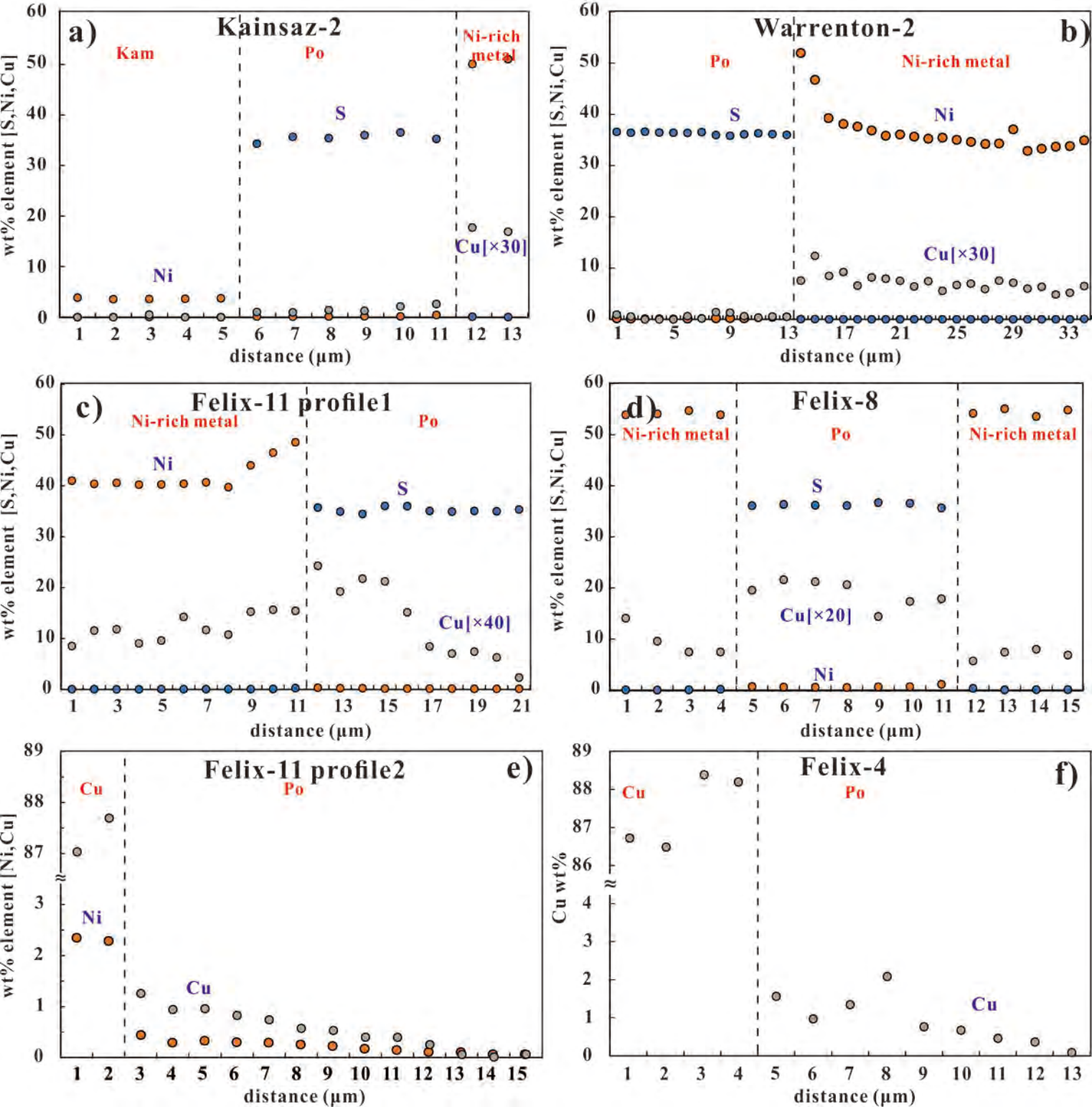
a)
Kainsaz-2
Kam
Po
Ni-rich metal
S
Ni
Cu[×30]
wt% element [S,Ni,Cu]
distance (μm)
b)
Warrenton-2
Po
Ni-rich metal
S
Ni
Cu[×30]
wt% element [S,Ni,Cu]
distance (μm)
c)
Felix-11 profile1
Ni-rich metal
Po
Ni
S
Cu[×40]
wt% element [S,Ni,Cu]
distance (μm)
d)
Felix-8
Ni-rich metal
Po
Ni-rich metal
S
Cu[×20]
Ni
wt% element [S,Ni,Cu]
distance (μm)
e)
Felix-11 profile2
Cu
Po
Ni
Cu
wt% element [Ni,Cu]
distance (μm)
f)
Felix-4
Cu
Po
Cu
Cu wt%
distance (μm)